

1 **Flood Risk Assessment and Increased Resilience for Coastal Urban**  
2 **Watersheds under the Combined Impact of Storm Tide and Heavy Rainfall**

3 Yawen Shen<sup>1</sup>, Mohamed M. Morsy<sup>2,3</sup>, Chris Huxley<sup>4</sup>, Navid Tahvildari<sup>5</sup>, Jonathan L. Goodall<sup>6,\*</sup>

4 <sup>1</sup>Graduate Research Assistant, Dept. of Engineering Systems and Environment, Univ. of Virginia, Olsson  
5 Hall, Charlottesville, VA 22904-4742, USA. E-mail: ys5dv@virginia.edu

6 <sup>2</sup>Research Associate, Dept. of Civil and Environmental Engineering, Univ. of Virginia, Olsson Hall,  
7 Charlottesville, VA 22904-4742, USA. E-mail: [mmm4dh@virginia.edu](mailto:mmm4dh@virginia.edu)

8 <sup>3</sup>Assistant Professor, Irrigation and Hydraulics Department, Faculty of Engineering, Cairo University,  
9 P.O. Box 12211, Giza 12613, Egypt

10 <sup>4</sup>Senior Engineer, BTM WBM Pty Ltd, Level 8, 200 Creek Street, Brisbane, 4000, Australia. E-mail:  
11 [chris.huxley@tuflow.com](mailto:chris.huxley@tuflow.com)

12 <sup>5</sup>Assistant Professor, Dept. of Civil and Environmental Engineering, Old Dominion University, Norfolk,  
13 VA 23529. E-mail: [ntahvild@odu.edu](mailto:ntahvild@odu.edu)

14 <sup>6</sup>Associate Professor, Dept. of Engineering Systems and Environment, Univ. of Virginia, Olsson Hall,  
15 Charlottesville, VA 22904-4742, USA. E-mail: [goodall@virginia.edu](mailto:goodall@virginia.edu)

16

17 \* corresponding author: E-mail: [goodall@virginia.edu](mailto:goodall@virginia.edu), phone: +1 (434) 243-5019

18 **Abstract**

19 Low-lying coastal cities are vulnerable to flooding under the combined impact of storm tide and heavy  
20 rainfall. While storm tide or heavy rainfall alone is able to directly cause widespread flooding in coastal  
21 areas, often heavy rainfall and storm tide happen concurrently, and the severity of flooding is greatly  
22 exacerbated. Current methods for understanding flood risk and mapping floodplains normally does not  
23 clearly communicate either the individual or combined impact of these two flooding mechanisms. Flood  
24 mitigation strategies typically target either rainfall-driven flooding (e.g., stormwater controls) or tidally-  
25 driven flooding (e.g., flood walls and tide gates). Thus, better understanding and communicating the  
26 individual and combined flood risk resulting from these two mechanisms can be important to improving  
27 flood resilience. To address this need, this study presents tools and methods for floodplain mapping in  
28 coastal urban environments where rainfall and storm tide driven flooding can be better understood and  
29 communicated. The approaches are demonstrated for a watershed in Norfolk, VA, USA as a case study  
30 system using a 1D pipe/2D overland flow hydrodynamic model built for the watershed. Storm tide and  
31 heavy rainfall events with return periods varying from 1 to 100-year were designed based on historical  
32 observations and combined into a series of compound storm scenarios. Then these compound storm  
33 scenarios were simulated using the hydrodynamic model for simulating flow through both the land  
34 surface and underground pipe network systems. Results show how the capacity of the drainage system,  
35 and therefore flood risk reduction, is sensitive to storm tide levels, even for less extreme events with a 1-  
36 year return period. The model also provides new insights into the role of stormwater infrastructure in  
37 exacerbating flooding risk within communities during high sea level conditions. Results demonstrate how  
38 dividing the floodplain into different regions based on the dominant flooding mechanism (rainfall vs.  
39 storm tide) makes it possible to better target mitigation strategies to improve flood resilience. To this end,  
40 a transition zone index (TZI) is presented to help decision makers identify the change from rainfall-driven  
41 to tide-driven flooding for locations within a watershed. Finally, we demonstrate how different flood  
42 mitigation strategies can be tested using this modeling approach to better understand their impact on

43 increasing flood resilience within the system for portions of the floodplain impacted by rainfall-driven  
44 and tidal-driven flooding.

45 **Author keywords:** Coastal City; Urban Hydrology; Coastal Flood Mapping; Storm Tide; Heavy  
46 Rainfall; 2D Hydrodynamic Modeling; Flood Resilience

47

## 48 **1. Introduction**

49 In the context of sea level rise and climate change, flooding is one of the most challenging issues facing  
50 coastal cities today (Hallegatte et. al., 2013; Woodruff et al., 2013). Coastal cities form a vital component  
51 of national and global economies; however, coastal cities and their economies are increasingly vulnerable  
52 to extreme storm events (Hanson et al., 2011). As a consequence of extreme storm events, flooding  
53 impacts on these low-lying, densely populated, and highly developed regions can be devastating (Gallien  
54 et al., 2014; Wahl et. al., 2015; Karamouz et al., 2017; Sadler et al., 2017; Bilskie and Hagen, 2018). In  
55 coastal cities, flooding is primary caused by two processes: surface runoff due to inland heavy rainfall and  
56 tidal flooding from extreme high tide (Dawson et al., 2008; Archetti et al., 2011; Xu et al. 2014; Wahl et.  
57 al., 2015). Heavy rainfall is more likely to cause severe flooding in urban areas with poorly functioning or  
58 insufficient stormwater infrastructure (Upadhyaya et. al., 2014; Yazdanfar and Sharma, 2015). In coastal  
59 cities, rainfall-driven stormwater collected by drainage system is designed to drain into the sea either by  
60 gravity-fed flow or pumping. However, during extreme high tide events, the drainage capabilities are  
61 greatly reduced with a worse situation of backward flow. Additionally, extreme high tide alone is able to  
62 directly cause widespread coastal flooding (Xu et. al., 2014; Castrucci and Tahvildari, 2018). Thus, if  
63 heavy precipitation and extreme high tide happen concurrently, the severity of flood can be greatly  
64 exacerbated (Zheng et al., 2013; Xu et al., 2014; Wahl et. al., 2015; Karamouz et al., 2015, 2017; Wu et  
65 al., 2018). The extreme high tide discussed in this study is in the form of storm tide, which is the total  
66 observed seawater level during a storm resulting from the combination of storm surge and the  
67 astronomical tide.

68 Prior studies have used statistical methods to explore the interdependence between storm tide and  
69 heavy rainfall and their combined impact on flood risk (Zheng et. al., 2013; Xu et al., 2014; Wahl et. al.,  
70 2015; Batten et al., 2017; Wu et al., 2018). Zheng et al. (2013) investigated the presence of the  
71 dependence between extreme rainfall and storm surge on Australian coastline using available rainfall and  
72 tide level observations. They found a statistically significant dependence with regional and seasonal  
73 variations for the majority of studied locations. Wahl et al. (2015) studied the likelihood of concurrent  
74 storm tide and heavy rainfall for major coastal cities in the contiguous United States. It was found that the  
75 probability of combined storms is higher for the Atlantic/Gulf coast relative to the Pacific coast.  
76 Meanwhile, in many of the focused cities, the number of compound events has increased greatly over the  
77 past century, and this trend may continue under the changing environment. Xu (2014) and Batten (2017)  
78 estimated the joint probability of storm tide and extreme rainfall in their study areas and proposed design  
79 guidance for future flooding preparedness. Specifically, Batten (2017), who worked on the same region,  
80 coastal of Virginia, USA, as the current study, showed that over 50% of the rainfall events happened  
81 when sea water level was higher than mean daily high tide. While statistical approaches are important for  
82 understanding risk, they are not able to identify specific areas within a coastal community vulnerable to  
83 flooding, nor are they able to quantify how modifications to the built environment, in the form of  
84 infrastructure improvements, can mitigate flooding risk. Physical models of the system are needed for  
85 these challenges.

86 Coupled one-dimension (1D) pipe and two-dimension (2D) overland flood models are an efficient  
87 way to simulate urban flooding and have been widely used for assessing urban flood risk (Leandro et al.,  
88 2009; Seyoum et al., 2012; Russo et al., 2015; Fan et al., 2017; Xu et al., 2017; Martins et al., 2018). In  
89 prior studies, 1D models (Ray et. al., 2011; Lian et. al., 2013; Bacopoulos et al., 2017; Karamouz et al.,  
90 2017) or 2D models (Karamouz et al., 2017; Silva-Araya et. al., 2017) have been used to investigate the  
91 combined impact of storm tide and extreme rainfall, but the combination of 2D/1D modeling approaches  
92 to simulate both overland flow and flow through stormwater drainage systems for coastal watersheds is

93 novel. Coastal regions are usually located in low-relief terrains with flat or mild slopes and a large amount  
94 of storage potential, especially in coastal cities with complex topography and a large number of artificial  
95 structures. Routing water in such regions is not as straightforward as in high-gradient regions since water  
96 does not always stay within river channels. In confined channels, 1D models are able to generate good  
97 estimation of flooding as long as the water remains in the channels (Marks et al., 2004; Leandro et al.,  
98 2009). However, for extreme storm events in urban environment, stormwater flow can easily overtops the  
99 curbs in the streets, and the direction of the flow may change dramatically. In such conditions, a 2D  
100 model is a more reliable tool for urban flood simulation. However, even though 2D models were used in  
101 Karamouz (2017) and Silva-Araya (2017), the underground drainage system was not considered in both  
102 studies. Underground drainage system is a key component of stormwater management infrastructure in  
103 coastal cities, and its efficiency could be greatly influenced by the downstream tidal boundary conditions  
104 (Archetti et al., 2011). Therefore, in order to simulate coastal city flooding in a realistic manner, flood  
105 models need to be capable of simulating the dynamics of flow on ground surface and pipe flow in  
106 underground drainage system, as well as the interaction between them. An effective way is to use a 1D  
107 pipe and 2D overland coupled model. Several commercial or open-source 1D/2D modeling system are  
108 available, such as, the Two-dimensional Unsteady Flow (TUFLOW) model (Syme, 2001), MIKE 21  
109 (Carr and Smith, 2006), XP-SWMM, Leandro (2016), and Wu (2017). Such modeling systems can  
110 support coastal flood mapping with the consideration of the individual and combined flood risk resulting  
111 from storm tide and heavy rainfall, and it can be important to improving flood resilience by testing the  
112 impact of different potential mitigation strategies.

113 In prior studies, geospatial information and hydrodynamic models have been used for  
114 understanding flood risk and mapping coastal floodplains (Wang et al., 2002; Karamouz et al., 2015;  
115 Karamouz et al., 2017; FEMA, 2018). However, these methods normally do not clearly communicate the  
116 mechanisms of flooding for specific locations. In other words, it is not clear if the flooding is caused by  
117 the individual or combined impact of storm tide and heavy rainfall. This is problem in part because flood

118 mitigation strategies typically target either rainfall-driven flooding (e.g., stormwater controls) or tidally-  
119 driven flooding (e.g., flood walls and tide gates). To assess flood risk across coastal landscapes, Bilskie  
120 and Hagen (2018) proposed a methodology to delineate coastal floodplains into three flood zones, tidal  
121 zone, hydrological zone, and transition zone, according to different driving forces of flooding. The  
122 transition zone is defined as an area susceptible to the interaction between tidal and rainfall-driven flooding.  
123 Application of this method to a flooding event in southeast Louisiana shows that the excess rainfall and  
124 storm surge interact nonlinearly and their compound effect is smaller than their superposition (Bilskie and  
125 Hagen, 2018). Their study area was primarily located in a rural area with no effect from underground  
126 stormwater drainage systems. The transition zone identified from their study is primarily located in a  
127 region relatively close to the shoreline, where the tide has a significant impact on flooding. However, in  
128 urban environments, the interaction between rainfall-driven flooding and tidal flooding exists on both the  
129 land surface and subsurface through stormwater pipeline drainage systems. Thus, the influence of storm  
130 tide is not limited to the near-shoreline region, but extends further inland as well.

131         The objective of the study is to develop methodologies to enhance the understanding of the  
132 coastal city flood risk and how flood mitigation strategies in improving flood resilience. A high-  
133 resolution, coupled 1D pipe/2D overland hydrodynamic model was built using the TUFLOW modeling  
134 system for a watershed within the Hague community of Norfolk, VA, USA. TUFLOW solves the full 2D  
135 depth averaged momentum and continuity equations for shallow water free surface flow, and incorporates  
136 the full functionality of the ESTRY one-dimensional (1D) hydrodynamic network (Syme 2001). This  
137 modeling system outputs detailed flooding information on both land surface and underground pipeline  
138 system, which allows one to assess flood risk and understand the contribution of flooding from individual  
139 or combined factors. The coastal floodplain mapping method proposed in Bilskie and Hagen (2018) was  
140 extended for a coastal urban watershed based 2D/1D flood model simulations. The spatial extent of the  
141 transition zone was identified using different combinations of storm tide and heavy rainfall events. We  
142 also introduce an index to represent the likelihood of a region being susceptible to the combined impact of

143 storm tide and heavy rainfall. The mapping strategy assists in understanding how flood mitigation  
144 approach reduces flooding risk resulting from rainfall and storm tide drivers. The 1D pipe/2D overland  
145 flood model is also a powerful tool to evaluate the efficiency of different flood mitigation strategies. As a  
146 demonstration, two flood mitigation methods are tested in this study. The methodologies developed in  
147 this study can aid city planners and stormwater engineers in other coastal communities to understand and  
148 improve flood resilience by targeting both rainfall and storm tide-driven flooding.

149 The remainder of the paper is organized as follows. The methodology section provides  
150 background information about the study domain and explains the urban flood model and design the storm  
151 scenarios used in the study. It also includes a description of how flood zones were determined within the  
152 floodplain mapping analysis and introduces the concept of a transition zone index (TZI). The results and  
153 discussion section explains the model evaluation, how the lag between the peak storm tide and rainfall  
154 was determined in the modeling scenarios, and flood risk determined by the model. The influence of  
155 storm tide on the underground stormwater drainage system is also explored, followed by the coastal  
156 floodplain mapping results and a brief exploration of how flood mitigation strategies could reduce the  
157 floodplain for the study watershed. The paper concludes with key findings along with possible future  
158 research to further advance the approach.

159

## 160 **2. Methodology**

### 161 *2.1 Study area*

162 Norfolk, Virginia, USA is the second most populous city in Virginia and the home of world's largest  
163 naval base. Norfolk is a highly urbanized and relatively flat community with nearly all areas below  
164 elevation 4.5m (North American Vertical Datum of 1988: NADV 88). The relative low elevations and  
165 tidal connections to the Chesapeake Bay place a significant percentage of the city at risk of tidal flooding.  
166 The tidal flooding risk is more serious under the threat of sea level rise (SLR) and land subsidence (Li et.  
167 al., 2013; Sadler et. al., 2017). The study domain is located in the Hague community of the Norfolk, VA

168 (Figure 1). The sources of spatial datasets used in this study are provided in Table 1. The study domain  
 169 has a total area of 3.7 km<sup>2</sup>, including total waterbody area of 0.1 km<sup>2</sup> and land area of 3.6 km<sup>2</sup>, in which  
 170 0.7 km<sup>2</sup> is building area. Ground surface elevation of the study domain varies from 0.3m to 4.2m with an  
 171 average of 2.6m (NAVD88).

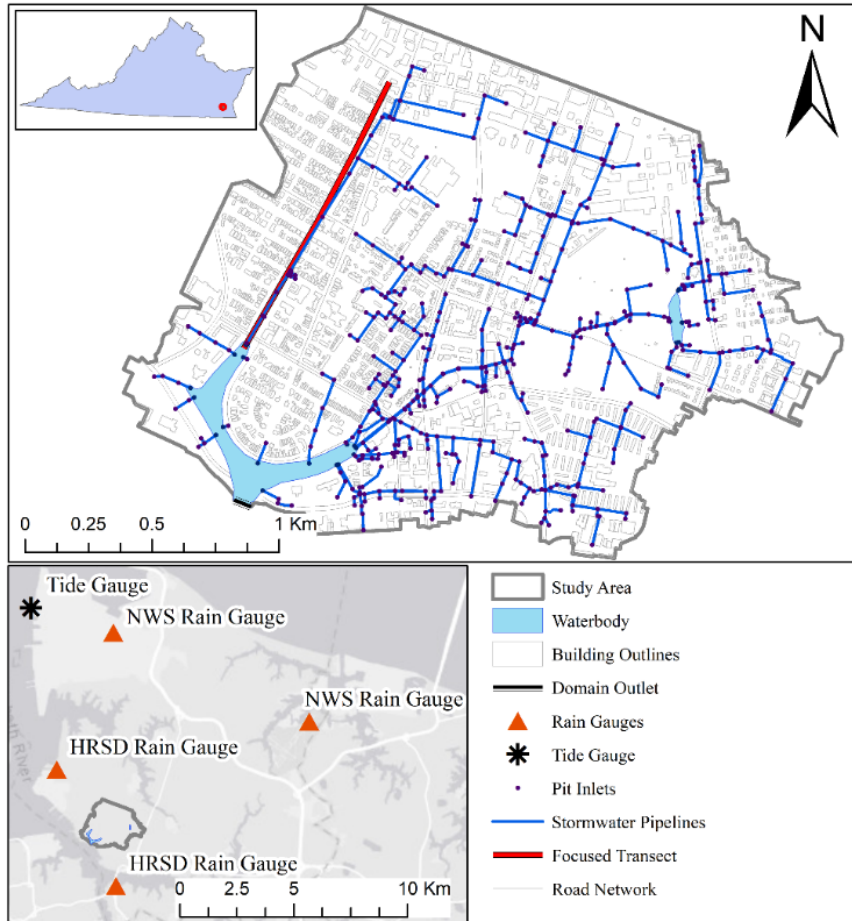
172 Table 1. Spatial Datasets Collected to Build the Urban Flood model

Spatial Dataset	Provider	Sources
LIDAR DEM	VGIN	<a href="https://www.vita.virginia.gov/integrated-services/vgin-geospatial-services/elevation---lidar/">https://www.vita.virginia.gov/integrated-services/vgin-geospatial-services/elevation---lidar/</a>
Land Cover	VGIN	<a href="https://www.vita.virginia.gov/integrated-services/vgin-geospatial-services/land-cover/">https://www.vita.virginia.gov/integrated-services/vgin-geospatial-services/land-cover/</a>
Basin Boundaries	Norfolk City	<a href="https://www.norfolk.gov/index.aspx?NID=1605">https://www.norfolk.gov/index.aspx?NID=1605</a>
Drainage System	Norfolk City	<a href="https://www.norfolk.gov/index.aspx?NID=1605">https://www.norfolk.gov/index.aspx?NID=1605</a>
Building Outlines	VGIN	<a href="https://www.arcgis.com/home/item.html?id=994d0afa44c046498f9774613671ce9a">https://www.arcgis.com/home/item.html?id=994d0afa44c046498f9774613671ce9a</a>
Road Centerlines	VGIN	<a href="https://www.vita.virginia.gov/integrated-services/vgin-geospatial-services/transportation/">https://www.vita.virginia.gov/integrated-services/vgin-geospatial-services/transportation/</a>

Note: VGIN: Virginia Geographic Information Network

173 In this study, the tide level data was collected from the Sewells Point station (Station ID:  
 174 8638610), which is 9.7km away from the domain tidal boundary. This tide gauge has the longest tide  
 175 level record, dating back to 1927, in Virginia. There is no official rain gauge located inside the study  
 176 domain. Rainfall data was obtained from two weather stations run by the U.S. National Weather Services  
 177 (NWS) and two other weather stations run by the Hampton Roads Sanitation District (HRSD) (Figure 1).  
 178 On average, the NWS and HRSD stations are about 9km and 3km away from the study domain center,  
 179 respectively. The two NWS weather stations have hourly rainfall data available since 1948 and 1973,  
 180 respectively. The HRSD stations were installed in January 2016. For hurricane events simulated the  
 181 study, the NWS rainfall record was used as rainfall input for hurricanes earlier than 2016, and the HRSD  
 182 rainfall record was used for hurricanes after 2016.





183

184

Fig. 1. Study area with tide gauge and rain gauge locations.

185 *2.2 The Urban Flood Model*

186 The study domain is located in a highly urbanized area with complex flow patterns and paths. The  
 187 interaction between overland flow and pipe flow significantly increases the complexity of flood modeling.

188 To overcome these difficulties, a 1D pipe/2D overland hydrodynamic flood model was built using the  
 189 TUFLOW model. TUFLOW was chosen due to its capability to represent surface flow on a 2D domain as  
 190 well as fluvial and pipe network via its 1D functionality and the dynamically link between the two. The  
 191 TUFLOW High-performance Computing (HPC) engine allows to execute the model on multiple GPU  
 192 units, which would significantly speed up model simulations.

193 The domain boundary was selected from the basin boundaries provided by the City of Norfolk,  
 194 and adjusted based on a high resolution LiDAR digital elevation model (DEM) and the underground  
 195 drainage system. There is no rainfall-driven flow, in the form of overland or pipe flow, entering into the  
 196 study domain from adjacent watersheds. Therefore, all rainfall-driven flooding is generated inside the  
 197 domain. The outlet of the domain connects to the Elizabeth River, which is a portion of the Chesapeake  
 198 Bay. Wave speed of tide is currently not considered in this study. So, the tide level at Swells Point was  
 199 considered to be the same as the outlet of the study watershed. The topography of the 2D domain was  
 200 defined using a  $1m \times 1m$  Lidar DEM, building outlines, and road centerlines collected from the Virginia  
 201 Geographic Information Network (VGIN), as shown in Table 1. A land cover dataset with 1m spatial  
 202 resolution was obtained from VGIN to define the overland roughness. The Manning's roughness  
 203 coefficients for overland flow from McCuen (1998) were assigned to the 2D domain based on the land  
 204 cover types, as shown in Table 2. For a small watershed, flooding is primarily from short-duration  
 205 extreme storm events (Bryndal et al., 2017). At the same time, the current study area has an  
 206 imperviousness ratio of 57% and shallow groundwater level. Thus, infiltration is expected to have minor  
 207 influence on flooding caused by extreme storm events. Therefore, infiltration was not considered in the  
 208 current version of the urban flood model, which presumes saturated conditions within the watershed prior  
 209 to the model simulation period.

210 Table 2. Parameters used in the 1D pipe/2D overland hydrodynamic model

Parameters	Type	Value
Manning's n value of 2D overland surface	Asphalt	0.012
	Concrete	0.013
	Other urban feature	0.012
	Grassland	0.15
	Shrub land	0.4
Manning's n value of 1D pipelines	Plastic pipes	0.012
	Concrete pipe	0.014
	Cast iron pipe	0.013
	Corrugated-metal pipe	0.015
	Brick	0.014

211 TUFLOW solves the full 2D depth averaged momentum and continuity equations for shallow  
212 water free surface flow, and incorporates the full functionality of the ESTRY one-dimensional (1D)  
213 hydrodynamic network (Syme 2001). In TUFLOW, inlets and grates are represented as pits, which allow  
214 modelers to specify a depth-discharge relationship between ponding depth at pits and flow rate entering  
215 drainage system. The depth-discharge relationship, controlled by the type and dimension of inlet, defines  
216 the flow rate of overland stormwater entering into the pipeline system. The urban drainage design  
217 manuals from Federal Highway Administration (2009) and state departments of transportation (e.g.:  
218 VDOT, 2017) provide methods to calculate the draining capacity corresponding to the type and  
219 dimensional of different inlets. In this study, the depth-discharge curves were determined for different  
220 types of inlets based on the VDOT Drainage Manual (2017). The initial pipeline entrance and exit energy  
221 loss coefficients are set as value of 0.5 and 1.0, respectively. TUFLOW is capable of automatically  
222 adjusting energy loss coefficients associated with the contraction and expansion of flow into and out of a  
223 structure according to the approach and departure velocities in the upstream and downstream channels.  
224 Details of the energy loss adjustment technique are included in TUFLOW manual (2016) and Tullis and  
225 Robinson (2008). The Manning's roughness coefficients were assigned to different types of pipelines, as  
226 shown in Table 2.

### 227 *2.3 Designing of Combined Storm Events*

228 This study focuses on storm tide and heavy rainfall occurring with hurricanes on the Virginia coastline. A  
229 summary of the hurricane history of central and eastern Virginia is provided by the National Weather  
230 Service (NWS, 2016). Flood risk as a consequence of storm tide and heavy rainfall with the return periods  
231 varying from 1 to 100-year are simulated and investigated in this study. Thus, hurricanes, resulted in both  
232 storm tide and rainfall with recurrence intervals less than one year for coastal Virginia, were filtered out  
233 from the list of hurricanes analyzed in this section. Historical hurricanes with rainfall and tide peak  
234 recurrence intervals greater than one year are listed in Table 3. Hourly rainfall data were collected from  
235 the NWS weather station 013737 due to it having the longest record in the study region. The Sewells

236 Points station was installed in 1927 to collect tide level data, thus only hurricanes happened after 1927 are  
 237 listed in Table 3. For the 15 hurricanes with an available rainfall record, the total amount of rainfall varies  
 238 from 16.8mm to 289.9mm. The minimal and maximum tide peaks are 0.55m and 1.95m (NAVD88),  
 239 respectively. The rainfall durations of the 15 hurricanes vary from 8 to 77 hours with the median of 22  
 240 hours. Ten out of the 15 hurricanes have rainfall durations between 16 to 30 hours. Therefore, because  
 241 rainfall events happening during hurricanes in the Virginia coastal region have average durations of about  
 242 22 hours. A 24-hour duration was selected as the design rainfall events in this study.

243 Table 3. Historical hurricanes in Virginia with return period of rainfall or storm tide greater than one year.

Year	Storm Event	Rainfall Duration (hrs)	Total Rainfall (mm)	Peak Tide Level (m, NAVD88)
1928	Unnamed	--	--	1.13
1933	Unnamed	--	--	1.95
1936	Unnamed	--	--	1.56
1953	Barbara	--	--	0.83
1960	Donna	22	109.6	1.22
1964	Cleo	24	289.9	0.55
1964	Dora	30	122.0	1.19
1971	Doria	22	78.6	0.61
1985	Gloria	18	143.6	1.04
1986	Charley	16	27.5	1.13
1998	Bonnie	14	92.8	1.20
1999	Floyd	33	166.5	1.29
2003	Isabel	8	16.8	1.91
2004	Charley	15	94.6	0.80
2006	Ernesto	27	256.6	1.19
2011	Irene	27	207.7	1.81
2012	Sandy	77	151.8	1.57
2016	Hermine	20	68.2	1.38
2016	Matthew	21	234.7	1.27

244

### 245 2.3.1 Designing of Storm Tide Events

246 The annual exceedance probability curves of extreme tide levels for the Sewells Points station were  
 247 generated by the U.S. National Oceanic and Atmospheric Administration (NOAA)

248 (<https://tidesandcurrents.noaa.gov/est/curves.shtml?stnid=8638610>). The annual exceedance probability

249 curves of extreme tide levels with 95% confidence intervals are included in the report. The curves were  
 250 calculated from the annual highest tide levels after the mean sea level trend was removed. The tide levels  
 251 with different return periods along with the 95% confidence intervals are obtained from the NOAA report  
 252 as shown in Table 4. The tide level was converted from the Mean Higher High Water (MHHW) datum to  
 253 NAVD88 to be consistent with the urban flood model settings.

254 Table 4. Annual exceedance probabilities and return periods of extreme tide levels and the matched  
 255 historical hurricanes.

Exceedance Probability		99% (1-Yr)	10% (10-Yr)	2% (50-Yr)	1% (100-Yr)
Tide Level (m, NAVD88)		0.78	1.56	1.87	2.06
95% Confidence Intervals		0.72 - 0.81	1.35 - 1.61	1.64 - 2.33	1.76 - 2.74
Historical Hurricanes	Name	Charley (2004)	Unnamed (1936)	Isabel (2003)	Unnamed (1933)
	Tide Peak Level (m)	0.8	1.56	1.91	1.95

256

257 The tide level time series observed during historical hurricanes are taken as the references for  
 258 designing storm tide events. Tide peak levels were selected as an indicator to choose historical hurricanes  
 259 as reference to design storm tide events. For storm tides with certain return periods in Table 4, the  
 260 matched hurricane events in Table 3 have tide peak levels that are close to the storm tide peaks and fall in  
 261 between the 95% confidence intervals. The tide level observations of the matched hurricanes would be  
 262 taken as the designed storm tide events. Take the 50-year storm tide event as an example. According to  
 263 Table 4, the 50-year tide has a peak of 1.87m (NAVD88) with 95% confidence intervals from 1.64m to  
 264 2.33m. In the Table 3, Hurricane Isabel (2003) had a tide level peak of 1.91m, which is closest to the 50-  
 265 year tide among all these hurricanes. At the same time, the tide peak level of Hurricane Isabel (2003) falls  
 266 in between the 95% confidence interval of the 50-year tide. Therefore, Hurricane Isabel (2003) was  
 267 selected as the 50-year storm tide event in this study, and its tide level observation was used to design the  
 268 50-year storm tide event. Designed storm tide events with return periods of 1, 10, 50, and 100 years are  
 269 presented in Figure 2.

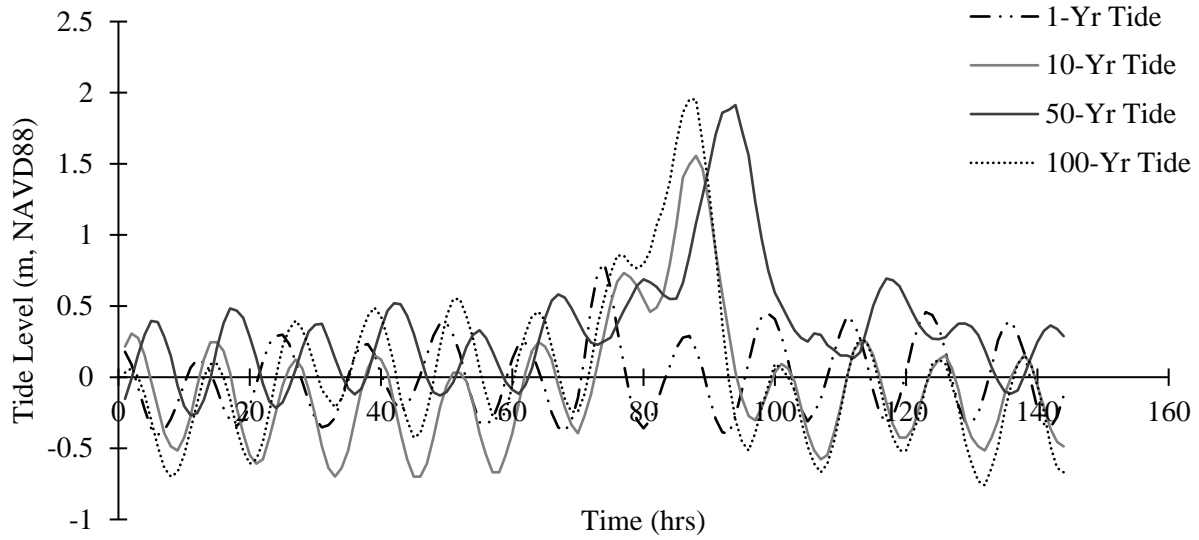


Fig. 2. Designed storm tide events with different return periods.

270  
271

272 2.3.2 Designing of Heavy Rainfall Events

273 In this study, the rainfall intensity-duration-frequency (IDF) curves were obtained from the NOAA Atlas  
 274 14 precipitation frequency estimates (Bonnin et. al., 2006). The NOAA Atlas 14 contains precipitation  
 275 frequency estimates with associated confidence intervals for the United States, and it is provided through  
 276 a web site ([https://hdsc.nws.noaa.gov/hdsc/pfds/pfds\\_map\\_cont.html](https://hdsc.nws.noaa.gov/hdsc/pfds/pfds_map_cont.html)). The 24-hour rainfall intensities  
 277 with the 90% confidence intervals for different return periods were obtained from the NOAA Atlas 14  
 278 and are shown in Table 5.

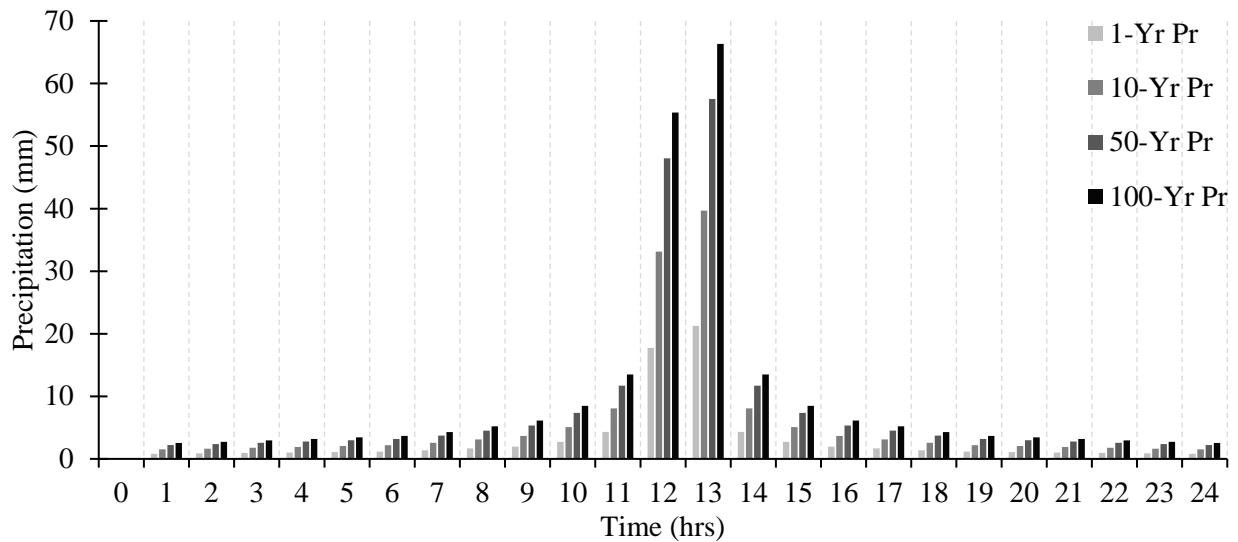
279 Table 5. NOAA Atlas 14 precipitation frequency estimates with 90% confidence intervals.

Exceedance Probability	99% (1-Yr)	10% (10-Yr)	2% (50-Yr)	1% (100-Yr)
24-Hr Rainfall Intensity (mm)	74	140	202	234
90% Confidence Intervals (mm)	69 - 81	129 - 152	183 - 218	210 - 253

280

281 The rainfall distribution used for rainfall design storms was obtained from a Natural Resources  
 282 Conservation Service (NRCS) study (Merkel et al., 2015). In Merkel’s study (2015), four types of rainfall  
 283 distributions were developed from data in the NOAA Atlas 14. A map showing a multistate area with  
 284 groups of regional precipitation distributions was presented along with tables containing 24-hour  
 285 precipitation distributions in Merkel’s study (2015). The current study domain is located in the region of

286 Type C precipitation distribution. The precipitation distribution is non-dimensional between values 0 to  
 287 1.0. Designed rainfall events were generated by multiplying the Type C precipitation distributions with  
 288 the corresponding 24-hour rainfall intensities from the NOAA Atlas 14. The synthetic rainfall events with  
 289 different return periods are presented in Figure 3.



290 Fig. 3. Synthetic 24-hour heavy rainfall events with different return periods.  
 291

292 A series of compound storm scenarios were created by combining different synthetic storm tide  
 293 and heavy rainfall events. The combined impact of storm tide and heavy rainfall are investigated  
 294 according to the urban flood model simulation for these storm scenarios. Flood simulations on both 2D  
 295 land area and 1D pipelines were generated as outputs.

#### 296 2.4 Determine Food Zones

297 According to Bilskie and Hagen (2018), the coastal floodplain can be separated into three different flood  
 298 zones, hydrological zone, tidal zone, and transition zone, based on the driving forces of flooding. In the  
 299 tidal zone, storm tide is the primary factor of flooding and rainfall has negligible impacts. The tidal zone  
 300 is usually located near a shoreline. The hydrological zone, normally located inland, is dominated by  
 301 rainfall-driven flooding with only minor impacts from storm tide. The transition zone is where significant  
 302 interactions exist between rainfall-driven and tidal flooding.

303            These three flood zones for a specific combined storm event are determined by the maximum  
304 water level simulations from three designed storm scenarios. In Simulation I, the storm tide is the only  
305 input, i.e., no rainfall input. Simulation II consists of heavy rainfall input with a normal tide. Normal tide  
306 means an average astronomical tide that cannot cause flooding in the study domain, and its maximum tide  
307 level is lower than all drainage pipeline outlets. Simulation III consists of both storm tide and heavy  
308 rainfall. Thus, flooding in Simulations I and II is driven by storm tide and rainfall, respectively, and it is  
309 driven by the combined effect of storm tide and rainfall in Simulation III. In the tidal zone, rainfall has  
310 negligible impacts on flooding; thus, the maximum water level simulation from Simulation III would  
311 have minor differences compared to Simulation I even with the existing of rainfall impact. Therefore, the  
312 tidal zone is defined as the area where the maximum water level simulations from Simulations I and III  
313 have a difference equal to or smaller than 0.01m. In the hydrological zone, storm tide has minor impacts  
314 on flooding. Therefore, the maximum water level simulations from Simulation II and III would be fairly  
315 close in the hydrological zone. In the current study, the hydrological zone is identified as the area where  
316 the maximum water level simulations from Simulation II and III have a difference equal to or smaller  
317 than 0.01m. The transition zone is normally located in between the hydrological and tidal zones. In the  
318 transition zone, both the maximum water level simulations from Simulation I and II are smaller than  
319 Simulation III with a difference greater than 0.01m.

320            The spatial extent of the transition zone varies with the change of storm tide and heavy rainfall  
321 combinations. Thus, simply mapping this zone does not fully describe this complex interaction between  
322 storm tide and heavy rainfall. In general, a greater tide peak or rainfall intensity would lead to a larger  
323 transition zone. For compound storms with higher tide peaks, the tidal zone and transition zone is more  
324 likely to extend further inland. Meanwhile, the increase of rainfall intensity would shrink the spatial  
325 extent of the tidal zone. To quantify this interaction, we defined the transition zone index (TZI) as

$$TZI = \frac{M}{N} \quad (1)$$



326 where,  $M$  is the number of simulations with transition zones sharing a same location, and  $N$  is the total  
327 number of simulations. TZI can be computed for any watershed based on the simulations from all the  
328 compound storm scenarios, as demonstrated in this study. A high TZI locates an area in the watershed  
329 where flooding is the product of interactions between storm tide and heavy rainfall. The higher the TZI,  
330 the stronger the interaction between these two primarily mechanisms for coastal flooding. TZI helps to  
331 identify regions in the watershed that would be impacted by flood mitigation approaches that target either  
332 storm tide driven flooding or rainfall driven flooding.

### 333 **3. Results and Discussion**

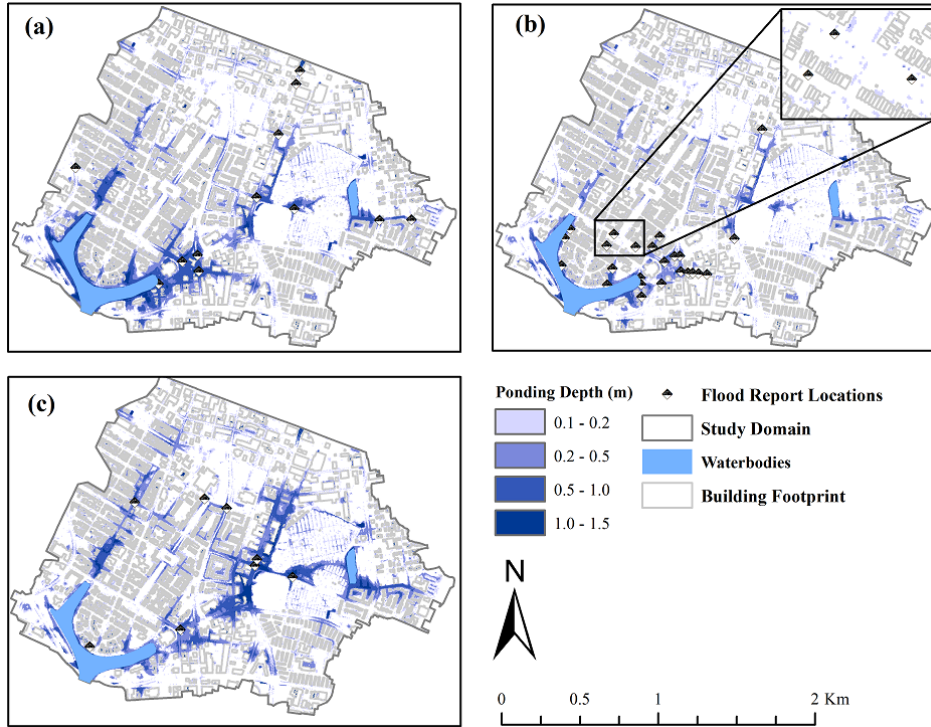
#### 334 *3.1 Model Evaluation*

335 Observations of the depth, extent, and duration of flooding in urban coastal landscapes are very rare;  
336 however, such data are essential to evaluate the performance of urban flood models (Smith et al., 2012).  
337 Data sources, such as photographs taken of flooded areas, newspaper reports and personal interviews,  
338 flood information collected from social media, and crowd-sourced drone footage, can be converted to  
339 inundation information for model evaluation (Smith et al., 2012; Middleton et al., 2014; Fohringer et al.,  
340 2015; Loftis et al., 2017). However, these data sources are often sparse and not available for the current  
341 study domain. In the current study, the data source used for flood model evaluation is a crowdsourced  
342 flood report dataset from the City of Norfolk, VA. This record includes flooded street locations in Norfolk  
343 starting from Hurricane Nicole on 30 September 2010 (Salder et al., 2018).

344 In the flood report record, only the date and location of reports were stored instead of the precise  
345 time and flood depth. Therefore, the maximum inundation maps on the date when flood locations were  
346 reported were compared with the flood report locations as an indication of model performance. During a  
347 storm event, stormwater may cause ponding on the most parts of the study domain. Ponding depth is  
348 selected as the indicator for inundation area mapping in this study. The inundation maps shown in this  
349 paper only include area with ponding depth greater than 0.1 m. This value was selected to distinguish

350 between dry land and flooded locations during storm events. It is assumed that the impact of flood is  
351 negligible for flood management purpose when the water depth is smaller than 0.1m.

352 The model performance was evaluated on Hurricanes Irene (2011), Hermine (2016), and Matthew  
353 (2016) (Figure 4). If simulated ponding exists in a 20m buffer of a flood reported location, this flood  
354 report was assumed to validate the model simulation. All flood reported locations of Hurricanes Irene and  
355 Matthew are consistent with the inundated areas from the simulations. During Hurricane Hermine, 25  
356 flood locations were reported, and 22 (88%) locations matched with the flood model simulation. The  
357 remaining three flood locations are about 250 m away from the shoreline as shown in Figure 4(b). The  
358 ponding depth at these three locations varies from 0.05 m to 0.09 m, which is lower than the cutoff depth  
359 selected for inundation area mapping. The crowdsourced flood report dataset contains unique and  
360 valuable street-level flood information, but there are still limitations of this dataset. As can be expected  
361 when using crowd-sourced data, the flood report dataset has an unknown amount of subjectivity and bias  
362 because the flood locations are reported by individuals (Sadler et al., 2018). Nonetheless, using the best  
363 available information, it is reasonable to suggest that the urban flood model has predictive skill at  
364 simulating flooded roads for three different extreme weather events.



365 Fig. 4. Ponding depth on time of maximum inundation area and flood report locations for hurricanes (a)  
 366 Irene (2011), (b) Hermine (2016), and (c) Matthew (2016)  
 367

368 *3.2 Time Lag between Storm Tide and Rainfall*

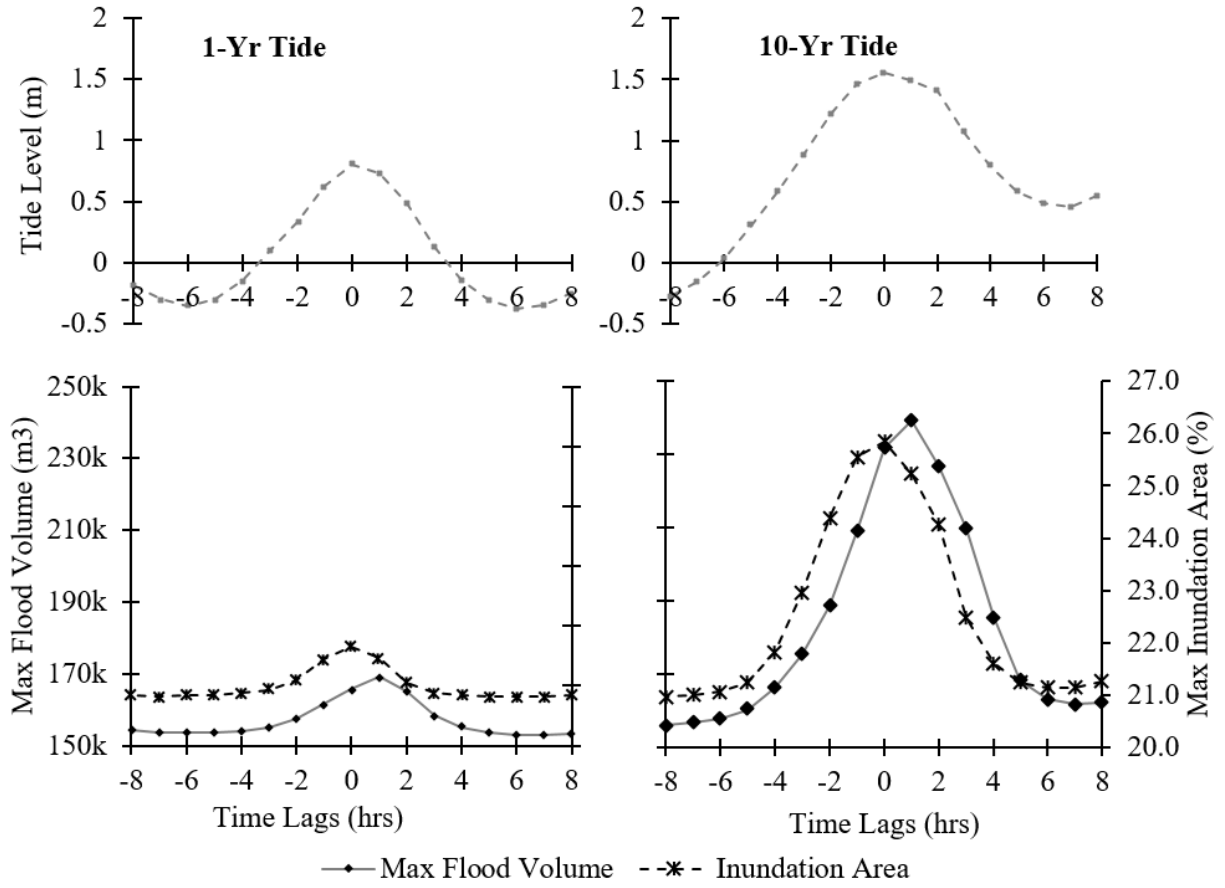
369 The storm scenarios were created by combining the synthetic rainfall and storm tide events; however, we  
 370 needed a method to match the time axis of rainfall and storm tide events. Usually, there is a time lag  
 371 between storm tide and rainfall events, and the time lag has a significant impact on flood risk (Zheng et  
 372 al., 2013). In this section, we show how the time lag between the tide peak and rainfall peak influence  
 373 flood risk in the study domain.

374 Time lag is defined as

$$T_{Lag} = T_{Tide Peak} - T_{Rainfall Peak} \quad (2)$$

375 where  $T_{Tide Peak}$  is the time of tide peak and the  $T_{Rainfall Peak}$  is the time of rainfall peak. In this  
 376 analysis, the 10-year rainfall is selected as an intermediate rainfall intensity. The 1 and 10-year storm  
 377 tides were chosen to represent a short duration (less than 6 hours) and a long duration (greater than 6  
 378 hours) storm tide, respectively. For each combination of storm tide and heavy rainfall, 17 synthetic storm

379 scenarios with time lags varying from -8 to 8 hours were created and simulated. The maximum inundation  
380 areas (MIA) in percentage of the total land area and the maximum flood volumes (MFV) on land are  
381 shown in Figure 5. The tide levels at the time of rainfall peak for each scenario are provided on the upper  
382 row of Figure 5. For both the 1-year tide and 10-year tide cases, the MIAs appear when tide peaks and  
383 rainfall peaks happen simultaneously, i.e., time lags equal to zero. The MFVs occur when rainfall peaks  
384 are one hour ahead of tide peaks (time lags equal to one). From Figure 5, we found that both MIA and  
385 MFV have positive correlations with tide levels at the time of rainfall peaks. When the absolute values of  
386 time lag are greater than 4 hours, rainfall peaks happen at low tide periods, and both MIA and MFV are  
387 relatively small. For scenarios with absolute values of time lag less than 4 hours, the MIA and MFV  
388 increase rapidly with the increase of tide levels at rainfall peaks. Using MIA and MFV as indicators, it the  
389 worst flooding appears to happens when the time lags are between -1 to 2 hours. In the current study, the  
390 compound storms with simultaneous storm tide and rainfall are chosen to represent the worst-case  
391 scenarios, where the worst-case scenarios are determined by using the MIA as the indicator of flood  
392 severity.



393  
 394 Fig. 5. Influence of time lag between storm tide and rainfall on flood risk with the examples of 10-year  
 395 rainfall event pairing with 1-year and 10-year storm tide events.

396 *3.3 Flood Risk*

397 The flood ponding depth at the time of maximum inundation area for each storm scenario is presented in  
 398 Figure 6. Among all storm scenarios, the maximum ponding depth of 1.49 m appeared during the  
 399 compound storm of 100-year rainfall and 100-year tide. For storm scenarios with fixed rainfall intensity,  
 400 for example, 1-year rainfall, the inundation area and ponding depth near the shoreline increase rapidly as  
 401 the storm tide return period increases. Several inland flood-prone areas are isolated from overland tidal  
 402 flooding; however, for a specific rainfall intensity, both the inundation area and ponding depth in these  
 403 areas experience a significant increase as the storm tide return period increases. Flooding in these flood-  
 404 prone areas are greatly influenced by the impact of storm tide on underground pipeline system, which will  
 405 be discussed in detail in the Section 3.5.

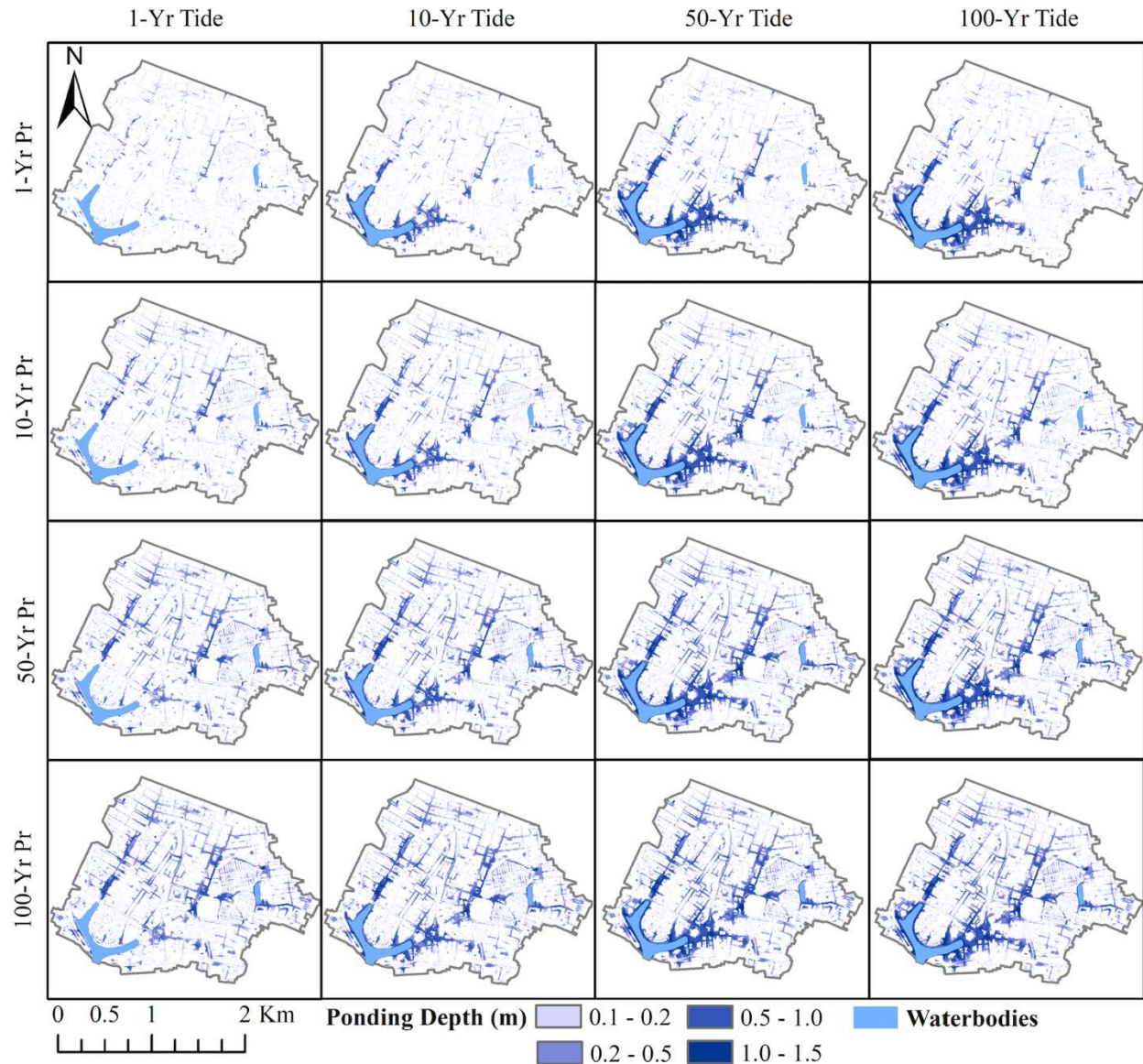


Fig. 6. Combined impact of storm tide and heavy rainfall on flood ponding depth at the time of maximum inundation area.

406  
407  
408

409

410

411

412

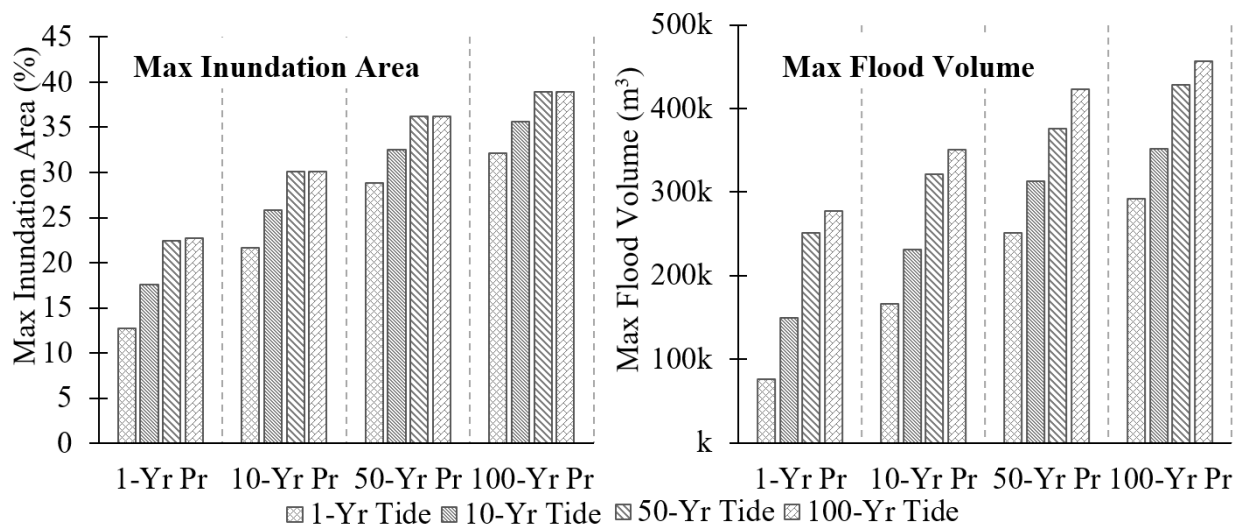
413

414

415

MIA and MFVs for different compound storm scenarios are provided in Figure 7. The storm scenario with the 1-year rainfall and 1-year storm tide would flood 12.7% of the land area with a MFV of about  $76,000m^3$ . The storm scenario with the 100-year rainfall and 100-year storm tide, according to the model, would cause MIA of 38.9% and MFV of about  $457,000m^3$ . From Figure 7, the results show that MIA is more sensitive to the change of rainfall return period compared to tide return period. For example, under the 1-year storm tide condition, MIA increases from 12.7% for 1-year rainfall to 32.1% for 100-year rainfall. In contrast, for the 1-year rainfall event, MIA increases from 12.6% to 22.7% for 1 and 100-

416 year storm tides, respectively. From Figure 7, MFV is susceptible to the change of both rainfall intensity  
 417 and storm tide severity. The simulations from certain storm scenarios have a similar amount of MIAs or  
 418 MFVs but different spatial extents. For example, the difference between MIAs for the storm scenario with  
 419 the 10-year rainfall and 1-year tide and the storm scenario with the 1-year rainfall and 50-year tide is only  
 420 0.7%. However, Figure 7 shows that these two scenarios, while having a similar MIA, have large  
 421 differences in the spatial extent of inundated areas. As expected, the flooded area of the event with a 1-  
 422 year rainfall and 50-year tide is primarily concentrated near the shoreline while the event with 10-year  
 423 rainfall and 1-year tide has flooded areas more inland with relatively shallow ponding depths.



424 Fig. 7. Maximum inundation area in percentage of land area and maximum flood volume on land for  
 425 different storm scenarios.  
 426

427 *3.4 Influence of Storm Tide on Underground Drainage System*

428 The study domain has a complex drainage system, which plays a key role in the stormwater management.  
 429 Model results and local knowledge of the drainage system both suggest that the efficiency of the drainage  
 430 system is highly sensitive to the tide levels at the outfalls. During storm tide events, the pipeline outfalls  
 431 can be partly or even fully submerged. In a submerged state, both the head difference between upstream  
 432 and downstream pipes and the capacity of the system are reduced, which slows the draining of stormwater  
 433 through the system.

434 In the study domain, the ground elevation of several roads and streets near the shoreline is higher  
435 than surrounding areas. These connected roads and streets form a barrier impeding overland tidal flooding  
436 entering into inland regions. The area in between the shoreline and these elevated roads and streets is  
437 defined as the shoreline floodplain. Inside the shoreline floodplain, inundation is the combined  
438 consequence of overland tidal flooding, local rainfall-driven flooding, and surcharge flow from the  
439 underground pipeline system. The inland region is free from overland tidal flooding. Thus, the inundation  
440 in the inland region is a consequence of local rainfall-driven flooding and surcharge flow from  
441 underground pipelines. Therefore, in the inland region, the flood severity for a fixed rainfall event is  
442 determined by the efficiency of the underground pipeline system, which is highly sensitive to the tide  
443 levels at outfalls. To explore the relationship between tide level and the efficiency of the drainage system,  
444 the flood severity in the inland region is analyzed under the impact of different storm tide events. In this  
445 section, the compound storm scenarios with 1-year rainfall and storm tide varying from normal tide to  
446 100-year tide were simulated and analyzed. Normal tide means an average astronomical tide that cannot  
447 cause flooding in the study domain, and its maximum tide level is lower than all drainage pipeline outlets.  
448 As shown in Figure 8, the maximum extent of the shoreline floodplain for these compound storm  
449 scenarios are covered by the shoreline floodplain mask, and the inland region is outside the mask. The  
450 focus pipes connect the inland region with the shoreline floodplain.



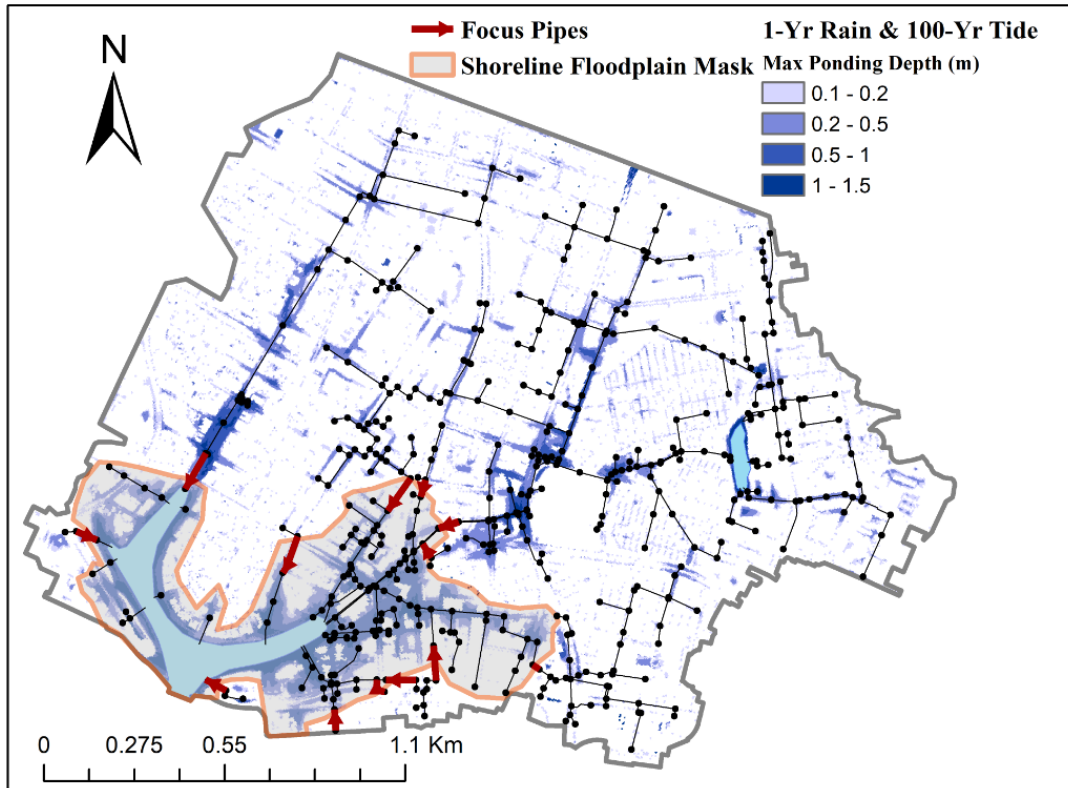


Figure 8. Locations of shoreline floodplain and focus pipes

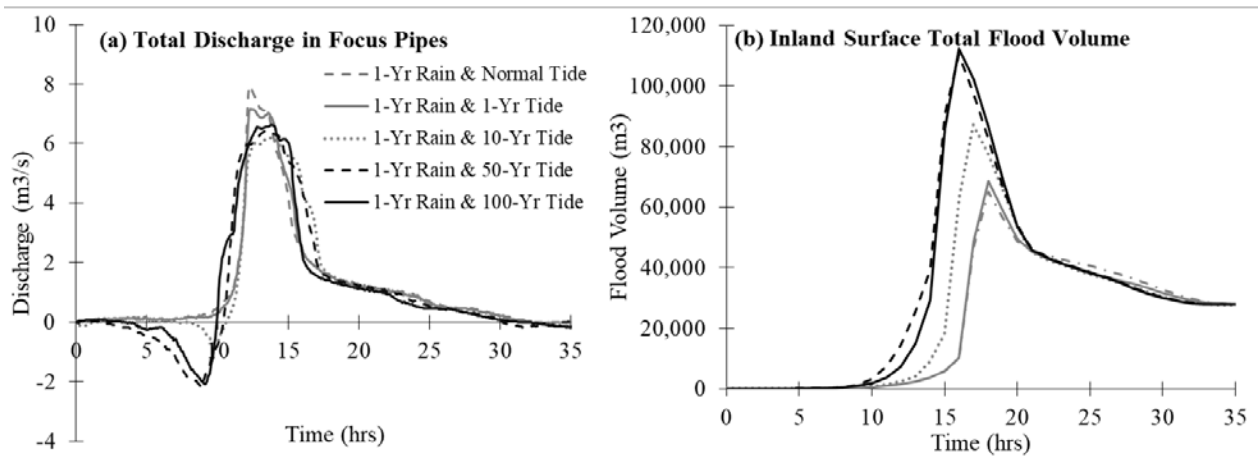
451  
452

453           The time series of total discharge in the focus pipes and the total amount of flood volume in the  
 454 inland region for the simulated compound storm scenarios are present in Figure 9. From Figure 9 (a),  
 455 there is no backward flow through the focus pipes under the normal tide and 1-year storm tide conditions.  
 456 Before hour 12, the total discharge time series have nearly identical trends under these two conditions.  
 457 However, the peak of total discharge under the 1-year storm tide condition is about 10% lower than the  
 458 normal tide condition. Meanwhile, from Figure 9 (b), the maximum inland flood volume for the 1-year  
 459 storm tide is about 5% higher than the normal tide. The pipeline outlets elevation is higher than the  
 460 normal tide peak, but lower than the 1-year storm tide peak. Therefore, the 1-year storm tide has a  
 461 blockage effect on the drainage system and would slow down the draining of inland stormwater.

462           When the recurrence intervals of storm tide are equal to or higher than 10 years, backward flow  
 463 would occur at the beginning period of the storms. This means these storm tide events are able to reach to  
 464 the pipelines in the inland region. Under the 10-year tide condition, the total volume of backward flow

465 through the focus pipes is  $37,000m^3$ . This volume would occupy a large portion of the storage space of  
 466 pipeline system and slow down the draining of runoff from the inland region. The blockage effect results  
 467 in the peak of total discharge under the 10-year tide condition decreased by 22% compared to the normal  
 468 tide condition, and the maximum inland flood volume increased by 34%.

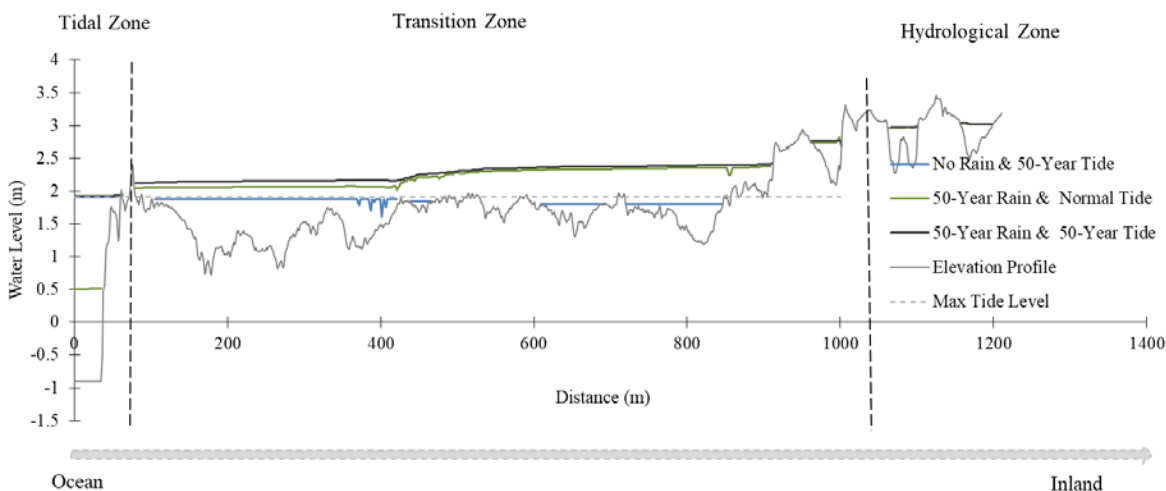
469 The total volumes of backward flow are  $310,000m^3$  and  $210,000m^3$  under the 50 and 100-year  
 470 storm tide conditions, respectively. In the current paper, designed storm tides are selected based on the  
 471 peak water levels; for example, the 100-year tide is 0.04m higher than the 50-year tide. However, the  
 472 duration of the 50-year tide is about 5 hours longer than the 100-year tide, which is the reason that the 50-  
 473 year tide caused greater volume of backward flow. The water head near the peaks of 50 and 100-year  
 474 storm tide events are higher than several flood-prone areas in the inland region. Thus, in the simulation, a  
 475 portion of the backward flow would exit the pipeline system and cause inundation in these areas. From  
 476 Figure 9 (b), the maximum flood volumes under the 50 and 100-year tide conditions have more than 70%  
 477 increase compared to the normal tide condition. Therefore, the surcharge flow on top of the blockage  
 478 effect on pipeline system greatly exacerbate the flooding in inland region.



479 Figure 9. Influence of tide level on the efficiency of the underground pipeline system: (a) total flood  
 480 volume of inland area under the condition of different storm tide scenarios; (b) total discharge in focus  
 481 pipes.  
 482

483 3.5 Coastal Floodplain Mapping

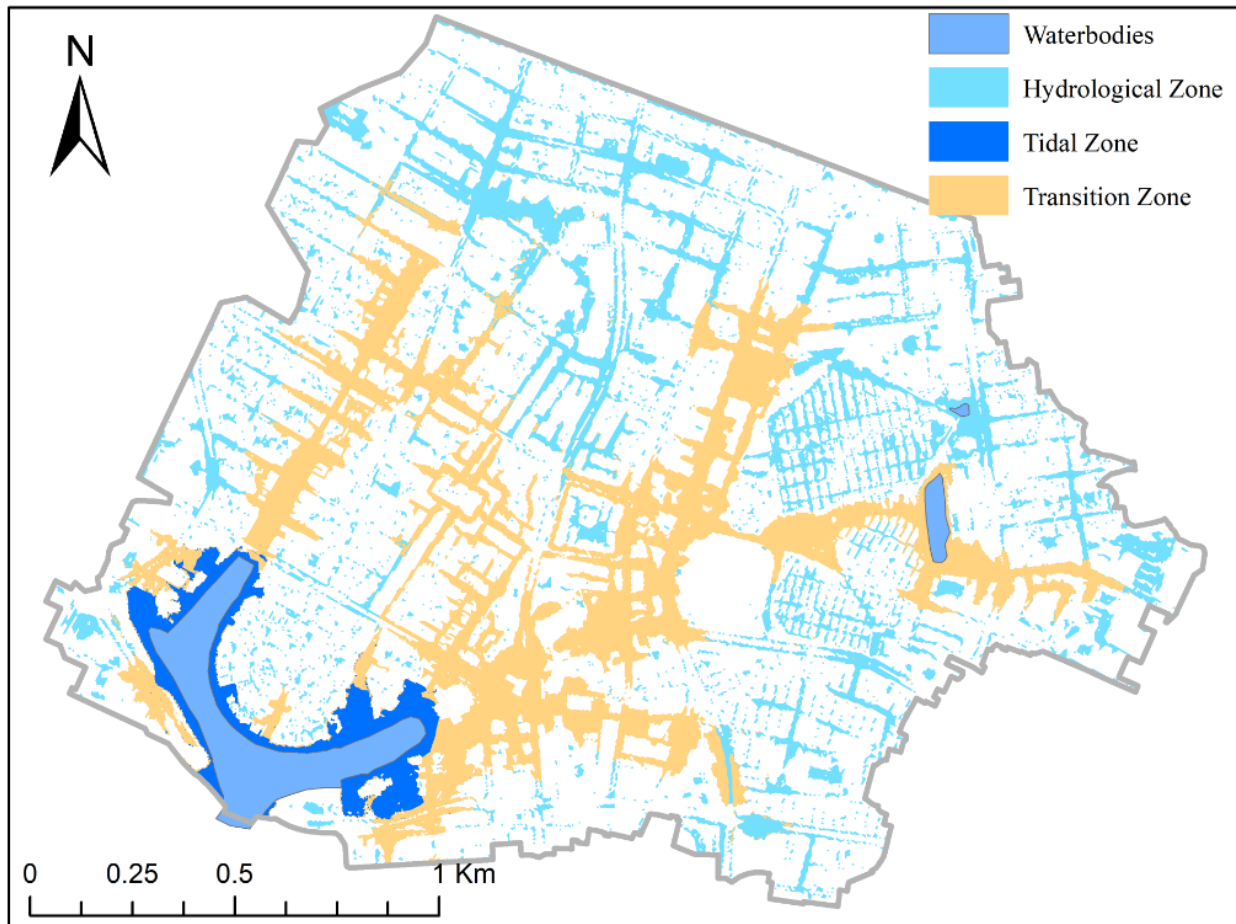
484 The coastal floodplain mapping method is demonstrated by three simulations generated from the  
485 50-year rainfall and 50-year storm tide. In Simulation I, the 50-year tide is the only input, i.e., no rainfall.  
486 Simulation II consists of 50-year rain and normal tide. Simulation III consists of 50-year rainfall and 50-  
487 year tide. For the focused transect in Figure 1, the maximum water level simulations for these three  
488 simulations, along with the land surface elevation profile, are presented in Figure 10. In the tidal zone, the  
489 maximum water levels from Simulations I and III have a difference less than 0.01m, which means the  
490 impact from rainfall is negligible. In the hydrological zone, the difference between maximum water level  
491 simulations from Simulations II and III is less than 0.01m. This indicates that storm tide has minor impact  
492 in the hydrological zone, and rainfall is the dominating factor. The transition zone is normally located  
493 between the tidal zone and hydrological zone. In transition zone, the maximum water level from  
494 Simulation III is higher than both Simulations I and II.



495  
496 Fig. 10. Land surface elevation profile and simulated maximum water levels across the selected transect for  
497 three storm scenarios.

498 For Simulation III, the spatial extent of different flood zones are identified, as shown in Figure 11.  
499 The total inundation area is  $1.17km^2$ , which is about 32.5% of the land area. The inundation area includes  
500 7% of the tidal zone, 43% of the hydrological zone, and 50% of the transition zone. The tidal zone is located  
501 in a narrow region near the shoreline. The hydrological zone is primarily distributed in inland region. The

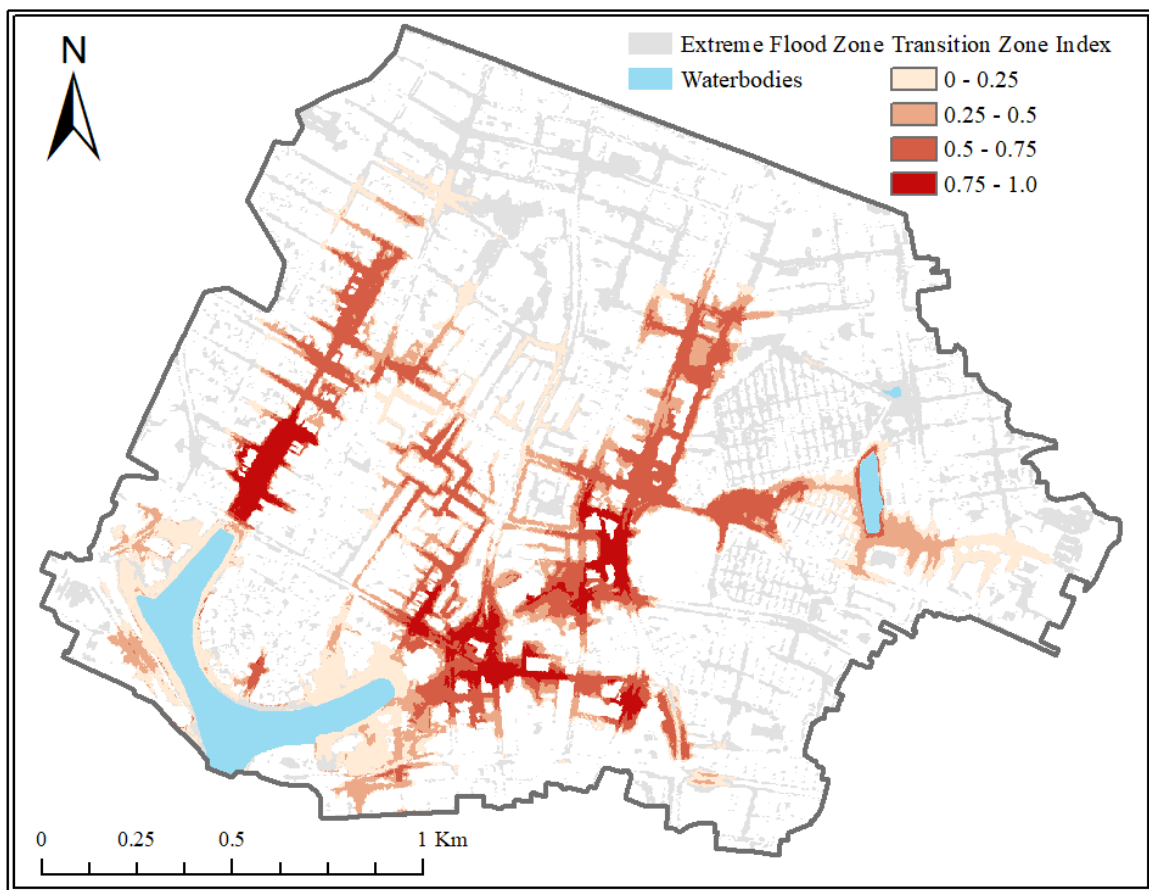
502 transition zone, as originally proposed by Bilskie and Hagen (2018), is located relatively close to the  
503 shoreline. However, in this study and in contrast to the Bilskie and Hagen (2018) study, due to the existing  
504 of pipeline system, the transition zone can reach to much further inland areas. This is because the strong  
505 interaction between rainfall-driven and tidal flooding exists for both the ground surface and underground  
506 drainage systems.



507  
508 Fig. 11. Flooding zones identified for storm scenario consists of 50-year storm tide and 50-year heavy  
509 rainfall

510 Based on the simulations from the 16 compound storm scenarios in this study, the transition zone  
511 index (TZI) was computed and presented in Figure 12. Generally, high TZI locates flood-prone areas  
512 where strong interaction exists between storm tide and heavy rainfall. These regions are prone to rainfall-  
513 driven flooding due to the relatively low elevation comparing to surround areas. Meanwhile, storm tide  
514 would slow down the draining of stormwater from these regions, and in extreme conditions, pipe flow can

515 become surcharge flow and exacerbate flooding severity. The high TZI areas are normally located in the  
516 middle region between shoreline and inland area. The inland region has zero or relatively small TZI,  
517 which means rainfall is the dominating factor of flooding. Thus, in the inland region, stormwater control  
518 measures (e.g., detention pond or rain garden) are effective flood mitigation strategies. In the near-  
519 shoreline region, storm tide is the primary driving factor of flooding because of the small TZI. Therefore,  
520 tide control measures (e.g., tide gates or flood walls) can be effective to reduce flood risk. For the high  
521 TZI areas, both stormwater and tide control measures can potentially help to reduce the flood risk, and the  
522 efficiency and mechanisms can be evaluated and explored using the 1D pipe/2D overland flood model.



523  
524 Fig. 12. Transition zone index estimated based on all compound storm scenario simulations

### 525 3.6 Flood Mitigation Strategies

526 In order to demonstrate how the model can be used to aid decision makers when decided between  
527 strategies for improving flood resilience within a system, two mitigation strategies were explored for the

528 case study watershed. In both cases, the TZI maps help decisions makers to anticipate regions within the  
529 watershed that will be improved based on the mitigation strategy selected. The first strategy is to install  
530 flap gates at certain locations within the drainage system to block backflow from high tide. This strategy  
531 is aimed at improving flood resilience for areas in the tidal zone with a low TZI value. The second  
532 strategy is to increase the useable capacity of a detention pond within the watershed to increase its  
533 capability for flood control. This strategy is targeted areas in the Hydrological Zone with low TZI value  
534 could be impacted by either of these two mitigation strategies in complex ways. The ponding depth  
535 reduction ratio is defined as the criteria for quantifying the improved resilience of the flood mitigation  
536 methods. The ponding depth reduction ratio is defined as

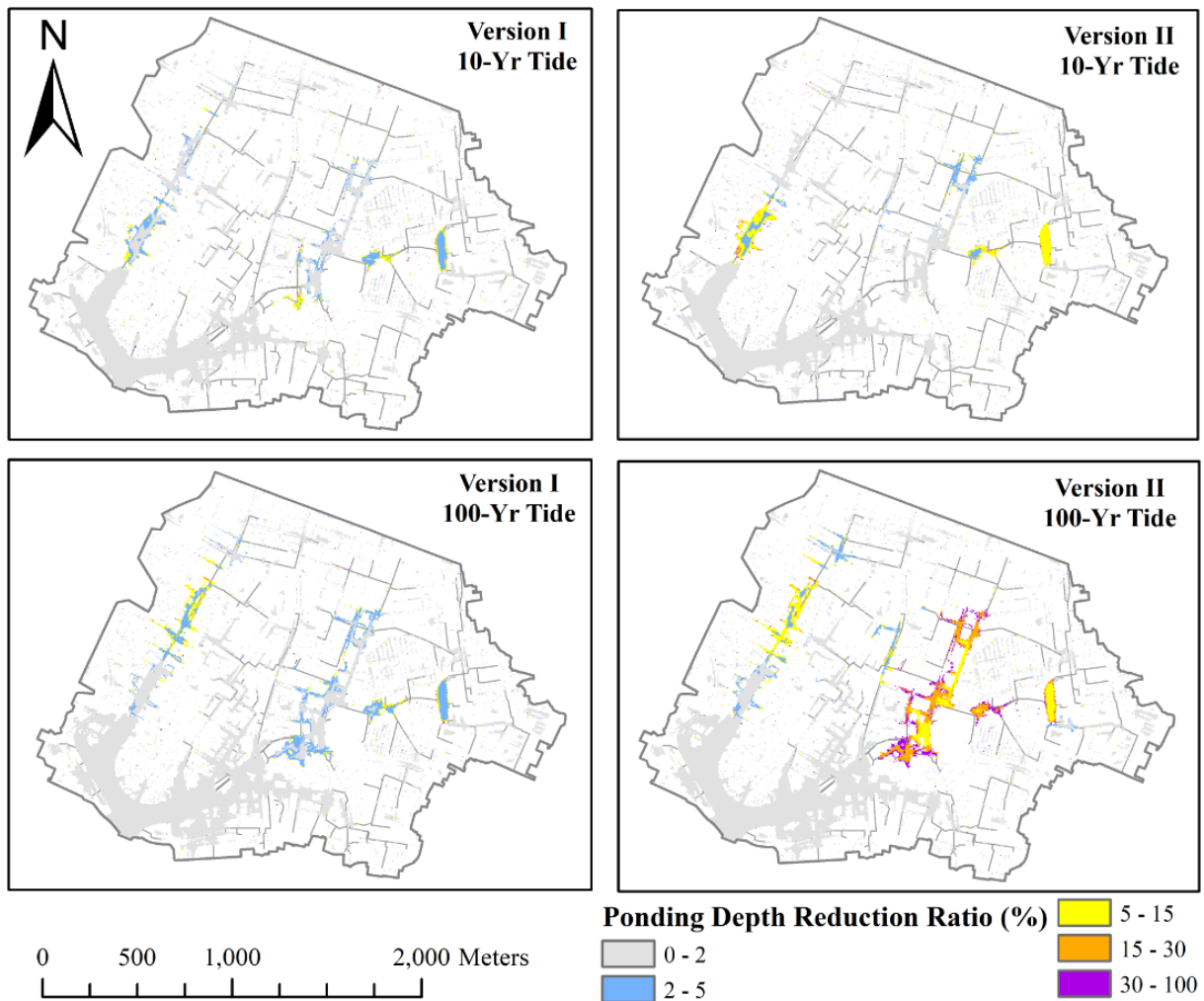
$$Ponding\ Depth\ Reduction\ Ratio = \frac{MPD_{Modified} - MPD_{Original}}{MPD_{Original}} \times 100\% \quad (3)$$

537 Where, the  $MPD_{Modified}$  is the maximum ponding depth simulation from the urban flood model  
538 including flood mitigation method, and the  $MPD_{Original}$  is the maximum ponding depth simulation from  
539 the original version of the urban flood model with no flood reduction measure.

540 Two methods of using flap gates are discussed in this section. The first method (Version I) is to  
541 install flap gates at the 17 outfalls of the drainage system. However, during extreme high tide, overland  
542 tidal flooding can reach to near-shoreline region to inundate several pits and manholes, and sea water  
543 would enter into the drainage system through these pits and manholes. The region inundated by overland  
544 tidal flooding is defined as the tidal floodplain. To further reduce the volume of backward flow from tide,  
545 the second method (Version II) is to install flap gates at all pipes covered by the 100-year tidal floodplain.  
546 The Version I and II methods were tested on storm scenarios with 1-year rainfall combined with 10 or  
547 100-year storm tide events. The maximum ponding depths were simulated from the urban flood models  
548 with and without flap gates. The ponding depth reduction ratio were calculated as shown in Figure 13.

549 Overall, the reduction of maximum ponding depth can be observed from the simulation in several  
550 flood-prone regions after flap gates are installed, also flap gates have greater influence for a more extreme

551 storm tide event. Under the combined impact of the 1-year rainfall and 10-year tide event, the Version I  
 552 method is able to reduce the ponding depth by 2% to 5% for several flood-prone areas, and 5% to 15% in  
 553 a small portion of these flood-prone area. Under the same event, the Version II method generates large  
 554 area with a reduction ratio between 5 to 15%. For the storm scenarios with 100-year tide, the ponding  
 555 depth reduction appear more expansive compared with the 10-year tide. However, the reduction ratio  
 556 from the Version I method is limited to the range of 2 to 15%, and the majority of that is between 2 to  
 557 5%. For the Version II method, the maximum ponding depth shows a significant reduction in the  
 558 upstream flood-prone area. In this case, a large area experiences a ponding depth reduction ratio between  
 559 5 to 30%, and several areas have a reduction ratio greater than 30%.



560

561 Fig. 13. Ponding depth reduction ratio between simulations with and without flap gates: (Version I) flap  
562 gates installed at drainage system outfalls; (Version II) flap gates installed in pipes inside the 100-year  
563 tidal floodplain. (Tested storm scenarios: 1-year rainfall with 10 and 100-year storm tide events).

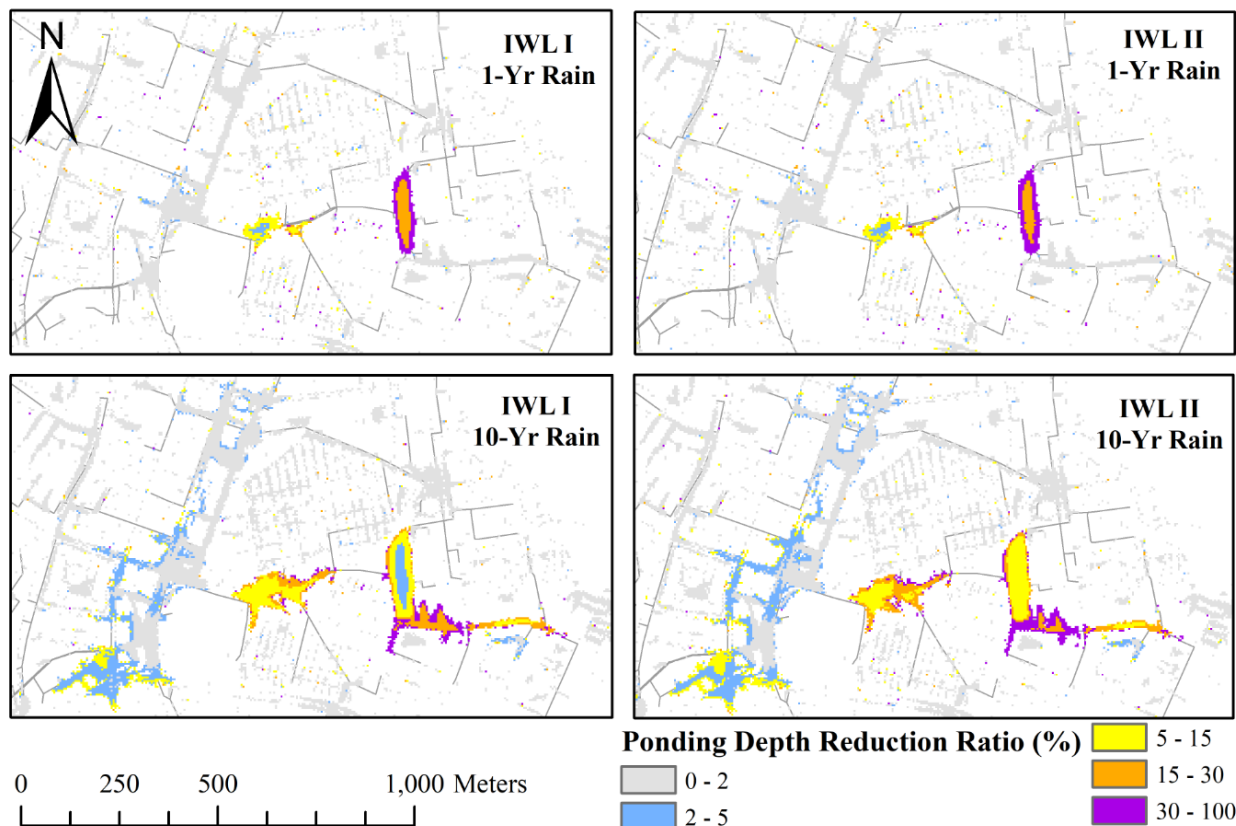
564 The detention pond in the study domain is a permanent pool of standing water that provides long-  
565 term water quality enhancement of stormwater runoff. Stormwater can also be temporarily stored in the  
566 detention pond for downstream flood control. The detention pond has a total capacity of about 24,000m<sup>3</sup>  
567 and a bed elevation of -1.83m (NAVD88). The detention pond has a normal water level of about 0.35m  
568 (NAVD88) and detention storage of about 15,600m<sup>3</sup>. The flood control ability of the detention pond is  
569 determined by its usable capacity at the beginning of storm events. To enlarge the usable capacity,  
570 stormwater control structures can be installed to lower the water level in advance of a forecasted storm.  
571 For example, if the water level is lowered to -1m (NAVD88), the detention pond would gain 7,000m<sup>3</sup>  
572 extra usable capacity for flood control.

573 Two initial water level (IWL) scenarios were tested in this section. For the first scenario (IWL I),  
574 the IWL was lowered to -1m above NAVD88. The second scenario (IWL II) had an IWL of -1.83m, the  
575 bed elevation, meaning the detention pond is dry under the IWL II condition. The IWL II is tested and  
576 discussed to represent a best-case scenario for flood risk reduction. The storm scenarios with the joint  
577 occurrences of 1 and 10-year rainfall with 1-year tide are selected to analyze the efficiency of flood  
578 mitigation when the detention pond is in IWL I and II conditions.

579 The ponding depth reduction ratios between the maximum ponding depth simulations with  
580 lowered IWLs and normal water level of the detention pond are calculated and presented in Figure 14.  
581 Generally, lowering the detention pond IWL only influences the flooding in local regions near the pond,  
582 and the ponding depth reduction ratios on IWL I and II conditions are very similar for both tested storm  
583 scenarios. This is because the usable capacities of the detention pond have relatively small difference  
584 (about 2,000m<sup>3</sup>) between IWL I and II conditions. With a 1-year rainfall event, the detention pond does  
585 not reach to its full capacity under both IWL conditions, and the maximum ponding depths in the region  
586 downstream the pond decrease by 2 to 15%. For a 10-year rainfall event, the detention pond does exceed



587 bankfull levels, and the maximum ponding depths in the downstream region near the pond decrease by 5  
 588 to 15%, and a portion of this region has more than a 15% ponding depth reduction ratio. A 2 to 15%  
 589 reduction ratio occurs in the further downstream. The most significant flood mitigation appears on the  
 590 southeastern portion of the detention pond drainage area due to increased capacity to store rainfall runoff  
 591 generated from this area.



592  
 593 Fig. 14. Ponding depth reduction ratio between the maximum ponding depth simulations on lowered  
 594 initial water levels and normal water level of the detention pond: (IWL I) initial water level lower to -1m;  
 595 (IWL II) initial water level lower to -1.84m. (Tested storm scenarios: 1 and 10-year rainfall with 1-year  
 596 tide event).

597  
 598 **4. Conclusions**

599 An overarching objective of this study was to develop methodologies to enhance the understanding of  
 600 flood risk within coastal urban watersheds. To this end, we modeled how overland flooding in an urban  
 601 watershed with stormwater drainage infrastructure is affected by storm tide and rainfall events with  
 602 varying return periods. The study area is located in Norfolk, VA, USA, a city prone to recurrent flooding

603 challenge, was the case study system for the study. The 1 to 100-year storm tide events were designed  
604 based on storm tides that happened during historical hurricanes impacting the Virginia coastline. A series  
605 of rainfall events with return periods varying from 1 to 100-year were designed based on the NOAA Atlas  
606 14 precipitation frequency estimates (Bonnin et. al., 2006). These design storm tide and rainfall events  
607 were combined to a series of compound storm scenarios. A coupled 1D pipe/2D overland hydrodynamic  
608 model was built for the study watershed using the TUFLOW model. The model outputs included detailed  
609 flooding information on both land surface and underground pipeline system, which allows to assess flood  
610 risk and understand the contribution of flooding from individual or combined factors. Floodplain maps  
611 and a new transition zone index (TZI) were created to communicate regions of the watershed under risk  
612 of flooding due to tide and rainfall-driven mechanisms. The 1D pipe/2D overland flood model and  
613 floodplain visualizations are a powerful tool to evaluate the efficiency of different flood mitigation  
614 strategies, as a demonstrated for two flood mitigation methods.

615         Results show how the capacity of stormwater drainage system is highly sensitive to storm tide  
616 levels. Based on model simulations, event with a 1-year tide is able to partially submerge the pipeline  
617 outlets and has an impact on the pipeline capacity. Storm tide events with return periods greater than or  
618 equal to 10 years would significantly reduce the drainage capacity. Extreme storm tide events, for  
619 example a 50 and 100-year tide, would cause flooding within the watershed due to the backing-up and  
620 day lighting of sea water traveling through stormwater drainage infrastructure. Even for smaller tide  
621 events, model simulations show that rainfall driven flooding combined with reduced capacity of the  
622 drainage infrastructure caused by tailwater conditions can cause significant flooding in inland regions.  
623 Due to the low gradient of the stormwater drainage infrastructure, which is common in many coastal  
624 urban areas, this interaction between rainfall-driven flow and sea water flow traveling through the pipe  
625 system can influence flooding far into the watershed.

626         This study provides a methodology that can be repeated for other coastal urban watersheds to  
627 better understand the influence of storm tide and rainfall-driven flooding through floodplain maps. The

628 coastal floodplain mapping method proposed in Bilskie and Hagen's study (2018) was applied to the  
629 urban watershed in the current study. In Bilskie and Hagen's study (2018), the study area is located in a  
630 rural area, and the interaction between rainfall-driving and tidal flooding is primarily within the region  
631 close to the shoreline. However, in this study, we extended on past work to include the stormwater  
632 drainage system, showing that the transition zone can reach much further inland due to the underground  
633 stormwater drainage system. The transition zone index (TZI) was defined to represent the likelihood of a  
634 location under the impact of strong interaction between tidal and rainfall-driven flooding. In areas with  
635 low TZI, flood risk is primarily caused by individual factors. Therefore, flood mitigation measures  
636 targeting to individual flood mechanisms can be effective ways to reduce flood risk in these parts of the  
637 watershed. For the high TZI areas, both stormwater and tide control measures can potentially assist to  
638 reduce the flood risk, and the efficiency and mechanisms can be evaluated and explored using the 1D  
639 pipe/2D overland flood model.

640       Lastly, the flood model and floodplain visualization is a powerful tool to evaluate the efficiency  
641 of different flood mitigation strategies. As a demonstration, two flood mitigation methods were tested in  
642 this study: one targeting rainfall-driven flooding and the second targeting tidal-driven flooding. The  
643 model simulations show how both methods would be able to reduce the flood risk for certain flood-prone  
644 regions of the watershed. Because the floodplain map helps to visualize regions of the watershed where  
645 tide, rainfall, or a combination of these two mechanisms cause flooding, it is easier to see how mitigation  
646 strategies improve flood resilience. This methodology can be of a significant value to cities and  
647 communities as they work to improve resilience for a host of services that can be impacted by flood risk.

648       The presented model will be used in a future study to explore several aspects of compound storm  
649 tide and rainfall-driven flooding. In this study, only tide level data is considered at the boundary as the  
650 tide input while tidal flow velocity may have a significant effect on tidal flooding and the function of  
651 drainage system. Future research should focus on coupling a hydrodynamic storm surge model with the  
652 inland hydrodynamic model to account for these processes. Furthermore, this study is focused on present

653 sea level. However, climate change impacts include increases in rainfall intensity and relative sea level  
654 rise (RSLR), which could substantially increase the severity of flood risk in the study area. Future  
655 assessments using this model will aim to quantify the impacts of changing climatic conditions on flooding  
656 risk.

657

## 658 **Acknowledgements**

659 This work was supported by the National Science Foundation under the award number 1735587. The  
660 authors wish to acknowledge the BMT for the TUFLOW HPC license and kindly help on model building  
661 and problem solving. We would also like to acknowledge the University of Virginia Advance Research  
662 Computing Services for providing the GPUs computing resource. NT acknowledges support from the  
663 Department of Transportation through Mid-Atlantic Transportation Sustainability-University  
664 Transportation Center (MATS-UTC).

665

## 666 **References**

667 Archetti, R., Bolognesi, A., Casadio, A., Maglionico, M., 2011. Development of flood  
668 probability charts for urban drainage network in coastal areas through a simplified joint  
669 assessment approach. *Hydrol. Earth Syst. Sci.* 15, 3115–3122. [https://doi.org/10.5194/hess-](https://doi.org/10.5194/hess-15-3115-2011)  
670 [15-3115-2011](https://doi.org/10.5194/hess-15-3115-2011).

671 Batten, B., Rosenberg, S., Sreetharan, M., 2017. Joint Occurrence and Probabilities of Tides and  
672 Rainfall. City of Virginia Beach. [https://www.vbgov.com/government/departments/public-](https://www.vbgov.com/government/departments/public-works/comp-sea-level-rise/Documents/joint-occ-prob-of-tides-rainfall-4-24-18.pdf)  
673 [works/comp-sea-level-rise/Documents/joint-occ-prob-of-tides-rainfall-4-24-18.pdf](https://www.vbgov.com/government/departments/public-works/comp-sea-level-rise/Documents/joint-occ-prob-of-tides-rainfall-4-24-18.pdf).

674 Bilskie, M. V, Hagen, S.C., 2018. Defining flood zone transitions in low-gradient coastal  
675 regions. *Geophys. Res. Lett.* 45, 2761–2770. [https://doi.org/https://](https://doi.org/https://doi.org/10.1002/2018GL077524)  
676 [doi.org/10.1002/2018GL077524](https://doi.org/10.1002/2018GL077524).

677 Bonnin, G.M., Martin, D., Lin, B., Parzybok, T., Yekta, M., Riley, D., 2006. NOAA Atlas 14  
678 Precipitation-Frequency Atlas of the United States. Silver Spring, Maryland.  
679 [http://www.nws.noaa.gov/oh/hdsc/PF\\_documents/Atlas14\\_Volume2.pdf](http://www.nws.noaa.gov/oh/hdsc/PF_documents/Atlas14_Volume2.pdf).

680 Bryndal, T., Franczak, P., Krocak, R., Cabaj, W., Kołodziej, A., 2017. The impact of extreme  
681 rainfall and flash floods on the flood risk management process and geomorphological  
682 changes in small Carpathian catchments: a case study of the Kasiniczanka river (Outer  
683 Carpathians, Poland). *Nat. Hazards* 88, 95–120. <https://doi.org/10.1007/s11069-017-2858-7>

- 684 Castrucci, L., Tahvildari, N., 2018. Modeling the Impacts of Sea Level Rise on Storm Surge  
685 Inundation in Flood-Prone Urban Areas of Hampton Roads, Virginia. *Mar. Technol. Soc. J.*  
686 52, 92–105. <https://doi.org/10.4031/MTSJ.52.2.11>.
- 687 Chen, A.S., Evans, B., Djordjević, S., Savić, D.A., 2012. A coarse-grid approach to representing  
688 building blockage effects in 2D urban flood modelling. *J. Hydrol.* 1–16.  
689 <https://doi.org/10.1016/j.jhydrol.2012.01.007>.
- 690 Dawson, R.J., Speight, L., Hall, J.W., Djordjevic, S., Savic, D., Leandro, J., 2008. Attribution of  
691 flood risk in urban areas. *J. Hydroinformatics* 10, 275.  
692 <https://doi.org/10.2166/hydro.2008.054>.
- 693 FEMA, 2018. Guidance for flood risk analysis and mapping: coastal general study  
694 considerations. <https://www.fema.gov/media-library/assets/documents/34953>.
- 695 Fohringer, J., Dransch, D., Kreibich, H., Schröter, K., 2015. Social media as an information  
696 source for rapid flood inundation mapping. *Nat. Hazards Earth Syst. Sci.* 15, 2725–2738.  
697 <https://doi.org/10.5194/nhess-15-2725-2015>.
- 698 Garcia, R., Restrepo, P., DeWeese, M., Ziemer, M., Palmer, J., Thornburg, J., Lacasta, A., 2015.  
699 Advanced GPU parallelization for two-dimensional operational river flood forecasting, in:  
700 In 36th International Association for Hydro-Environment Engineering and Research World  
701 Congress. The Hague, Netherlands.
- 702 Hallegatte, S., Green, C., Nicholls, R.J., Corfee-Morlot, J., 2013. Future flood losses in major  
703 coastal cities. *Nat. Clim. Chang.* 3, 802–806. <https://doi.org/10.1038/nclimate1979>.
- 704 Hanson, S., Nicholls, R., Ranger, N., Hallegatte, S., Corfee-Morlot, J., Herweijer, C., Chateau, J.,  
705 2011. A global ranking of port cities with high exposure to climate extremes. *Clim. Change*  
706 104, 89–111. <https://doi.org/10.1007/s10584-010-9977-4>.
- 707 Hunter, N.M., Bates, P.D., Neelz, S., Pender, G., Villanueva, I., Wright, N.G., Liang, D.,  
708 Falconer, R.A., Lin, B., Waller, S., Crossley, A.J., Mason, D.C., 2008. Benchmarking 2D  
709 hydraulic models for urban flooding. *Proc. Inst. Civ. Eng. - Water Manag.* 161, 13–30.  
710 <https://doi.org/10.1680/wama.2008.161.1.13>.
- 711 Huxley, C., Syme, B., 2016. TUFLOW GPU-best practice advice for hydrologic and hydraulic  
712 model simulations. in: *Proceedings of the 37th Hydrology and Water Resources Symposium*  
713 (HWRS). Queenstown, New Zealand.
- 714 Karamouz, M., Razmi, A., Nazif, S., Zahmatkesh, Z., 2017. Integration of inland and coastal  
715 storms for flood hazard assessment using a distributed hydrologic model. *Environ. Earth*  
716 *Sci.* 76, 1–17. <https://doi.org/10.1007/s12665-017-6722-6>

- 717 Karamouz, M., F., Zahmatkesh, Z., Goharian, E., S.M., Nazif, S., 2015. Combined Impact of  
718 Inland and Coastal Floods : Mapping Knowledge Base for Development of Planning  
719 Strategies 141, 1–16. [https://doi.org/10.1061/\(ASCE\)WR.1943-5452.0000497](https://doi.org/10.1061/(ASCE)WR.1943-5452.0000497).
- 720 Li, H., Lin, L., Burks-Copes, K.A., 2013. Modeling of coastal inundation, storm surge, and  
721 relative sea-level rise at Naval Station Norfolk, Norfolk, Virginia, U.S.A. *J. Coast. Res.* 29,  
722 18–30. <https://doi.org/10.2112/JCOASTRES-D-12-00056.1>.
- 723 Lian, J.J., Xu, K., Ma, C., 2013. Joint impact of rainfall and tidal level on flood risk in a coastal  
724 city with a complex river network: A case study of Fuzhou City, China. *Hydrol. Earth Syst.*  
725 *Sci.* 17, 679–689. <https://doi.org/10.5194/hess-17-679-2013>.
- 726 Loftis, J.D., Wang, H., Forrest, D., Rhee, S., Nguyen, C., 2017. Emerging flood model validation  
727 frameworks for street-level inundation modeling with StormSense, in: *Proceedings of the*  
728 *2nd International Workshop on Science of Smart City Operations and Platforms*  
729 *Engineering*. Pittsburgh, PA, pp. 13–18. <https://doi.org/10.1145/3063386.3063764>.
- 730 Mark, O., Weesakul, S., Apirumanekul, C., Aroonnet, S. B., and Djordjević, S., 2004. Potential  
731 and limitations of 1D modeling of urban flooding. *J. Hydrol. (Amsterdam)*, 299(3–4), 284–  
732 299.
- 733 McCuen, R.H., 1998. *Hydrologic Analysis and Design*, Second. ed, Prentice Hall. New Jersey.  
734 ISBN: 9786468600.
- 735 Merkel, W.H., Moody, H.F., Quan, Q.D., 2015. Design rainfall distributions based on NOAA  
736 Atlas 14 rainfall depths and durations. Beltsville, MD.  
737 [https://www.wcc.nrcs.usda.gov/ftpref/wntsc/H&H/rainDist/FIHMC\\_2015\\_Rainfall\\_Distrib](https://www.wcc.nrcs.usda.gov/ftpref/wntsc/H&H/rainDist/FIHMC_2015_Rainfall_Distribution_NOAA_14_Merkel.pdf)  
738 [ution\\_NOAA\\_14\\_Merkel.pdf](https://www.wcc.nrcs.usda.gov/ftpref/wntsc/H&H/rainDist/FIHMC_2015_Rainfall_Distribution_NOAA_14_Merkel.pdf).
- 739 Middleton, S.E., Middleton, L., Modafferi, S., 2014. Real-time crisis mapping of natural  
740 disasters using social media. *Soc. Intell. Technol.* 29, 9–17.  
741 <https://doi.org/10.1109/MIS.2013.126>.
- 742 Morsy, M.M., Goodall, J.L., O’Neil, G.L., Sadler, J.M., Voce, D., Hassan, G., Huxley, C., 2018.  
743 A cloud-based flood warning system for forecasting impacts to transportation infrastructure  
744 systems. *Environ. Model. Softw.* 107, 231–244.  
745 <https://doi.org/10.1016/j.envsoft.2018.05.007>.
- 746 NWS, 2016. The hurricane history of central and eastern Virginia.  
747 <https://www.weather.gov/media/akq/miscNEWS/hurricanehistory.pdf>
- 748 Ray, T., Stepinski, E., Sebastian, A., Bedient, P.B., 2011. Dynamic modeling of storm surge and  
749 inland flooding in a Texas coastal floodplain. *J. Hydraul. Eng.* 137, 1103–1110.  
750 [https://doi.org/10.1061/\(ASCE\)HY.1943-7900.0000398](https://doi.org/10.1061/(ASCE)HY.1943-7900.0000398).

- 751 Sadler, J.M., Goodall, J.L., Morsy, M.M., Spencer, K., 2018. Modeling urban coastal flood  
752 severity from crowd-sourced flood reports using Poisson regression and Random Forest. *J.*  
753 *Hydrol.* 559, 43–55. <https://doi.org/10.1016/j.jhydrol.2018.01.044>.
- 754 Sadler, J.M., Haselden, N., Mellon, K., Hackel, A., Son, V., Mayfield, J., Blase, A., Goodall,  
755 J.L., 2017. Impact of sea-level rise on roadway flooding in the Hampton Roads Region,  
756 Virginia. *J. Infrastruct. Syst.* 23, 05017006. [https://doi.org/10.1061/\(ASCE\)IS.1943-555X.0000397](https://doi.org/10.1061/(ASCE)IS.1943-555X.0000397).
- 758 Silva-Araya, W.F., Santiago-Collazo, F.L., Gonzalez-Lopez, J., Javier Maldonado-Maldonado,  
759 2018. Dynamic modeling of surface runoff and storm surge during hurricane and tropical  
760 storm events. *Hydrology* 5, 1–28. <https://doi.org/10.3390/hydrology5010013>.
- 761 Smith, R.A.E., Bates, P.D., Hayes, C., 2012. Evaluation of a coastal flood inundation model  
762 using hard and soft data. *Environ. Model. Softw.* 30, 35–46.  
763 <https://doi.org/10.1016/j.envsoft.2011.11.008>.
- 764 Svensson, C., Jones, D.A., 2004. Dependence between sea surge, river flow and precipitation in  
765 south and west Britain. *Hydrol. Earth Syst. Sci.* 8, 973–992. <https://doi.org/10.5194/hess-8-973-2004>.
- 767 Syme, W.J., 2008. Flooding in Urban Areas-2D Modelling Approaches for Buildings and  
768 Fences, in: 9th National Conference on Hydraulics in Water Engineering. Darwin City,  
769 Australia, pp. 23–26.
- 770 Syme, W.J., 2001. TUFLOW—Two & one-dimensional Unsteady FLOW Software for Rivers,  
771 Estuaries and Coastal Waters, in: Paper Presented at the IEAust Water Panel Seminar and  
772 Workshop on 2d Flood Modelling. Sydney, Australia, pp. 2–9.
- 773 Upadhyaya, J.K., Biswas, N., Tam, E., 2014. A review of infrastructure challenges: assessing  
774 stormwater system sustainability. *Can. J. Civ. Eng.* 41, 483–492.  
775 <https://doi.org/10.1139/cjce-2013-0430>.
- 776 Wahl, T., Jain, S., Bender, J., Meyers, S.D., Luther, M.E., 2015. Increasing risk of compound  
777 flooding from storm surge and rainfall for major US cities. *Nat. Clim. Chang.* 5, 1093–  
778 1097. <https://doi.org/10.1038/nclimate2736>.
- 779 Wang, Y., Colby, J. D., Mulcahy, K. A., 2002. An efficient method for mapping flood extent in a  
780 coastal floodplain using Landsat TM and DEM data. *International Journal of Remote*  
781 *Sensing.* 23 (18), 3681–3696. <https://doi.org/10.1080/01431160110114484>
- 782 Woodruff, J.D., Irish, J.L., Camargo, S.J., 2013. Coastal flooding by tropical cyclones and sea-  
783 level rise. *Nature* 504, 44–52. <https://doi.org/10.1038/nature12855>.

- 784 Xu, K., Ma, C., Lian, J., Bin, L., 2014. Joint probability analysis of extreme precipitation and  
785 storm tide in a coastal city under changing environment. PLoS One 9.  
786 <https://doi.org/10.1371/journal.pone.0109341>.
- 787 Yazdanfar, Z., Sharma, A., 2015. Urban drainage system planning and design - Challenges with  
788 climate change and urbanization: A review. Water Sci. Technol. 72, 165–179.  
789 <https://doi.org/10.2166/wst.2015.207>.
- 790 Zheng, F., Westra, S., Sisson, S.A., 2013. Quantifying the dependence between extreme rainfall  
791 and storm surge in the coastal zone. J. Hydrol. 505, 172–187.  
792 <https://doi.org/10.1016/j.jhydrol.2013.09.054>.

793

794

795

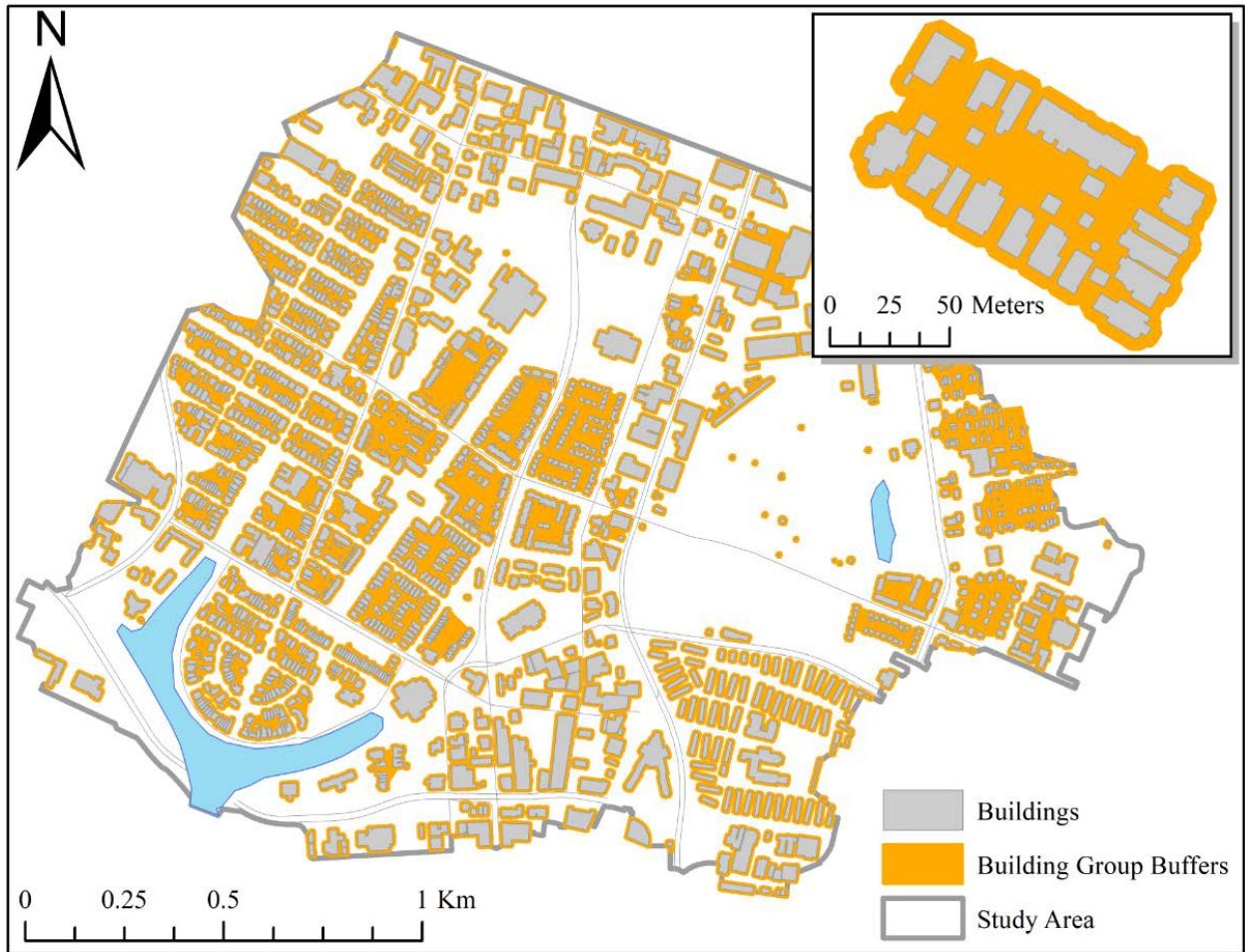
796

## 797 **Appendix A**

798 The watershed is urbanized and flow has complex patterns and paths through building areas.  
799 These buildings dissipate energy by forcing the flow to change its direction and speed. In prior studies,  
800 the buildings in the 2D model domain have been represented by increasing the roughness coefficient,  
801 blocking out of buildings, applying energy loss coefficient in building areas, and setting the buildings as  
802 porous elements (Hunter et. al., 2008; Syme, 2008; Chen et. al., 2012). In this study, one assumption is  
803 that no water would enter into buildings during simulations. Therefore, the method of blocking out of  
804 buildings is the only satisfactory option based on this assumption. As shown in Figure A1, the areas  
805 inside building outlines are deactivated from the 2D domain. To make sure no stormwater from rainfall  
806 lost by deactivating the buildings areas, a building representation method is proposed in this study,  
807 including three major steps: I) deactivate areas inside building outlines from the 2D domain; II) build  
808 polygons that includes groups of buildings; and III) apply the rainfall falling on the building areas to the  
809 buffered polygon around each group of buildings. The building roofs are designed to drain rain water  
810 rapidly and completely. The assumption behind the building representation method is that rain water can  
811 drain out of building roofs without any loss of rain water and no delay time from transferring the water



812 from precipitation to ground. This method is reasonable for the study domain where most of its buildings  
813 are residential houses with relatively small roof areas.



814  
815

Fig. A1. Representation of buildings in the urban flood model.

816